Order Number 9130299

Theoretical interpretation and calculation of the European muon collaboration effect

Cao, Nanwei, Ph.D.

City University of New York, 1991

U·M·I
300 N. Zeeb Rd.
Ann Arbor, MI 48106

THEORETICAL INTERPRETATION AND CALCULATION OF THE EUROPEAN MUON COLLABORATION EFFECT

By

NANWEI CAO

A dissertation submitted to the Graduate Faculty in Physics in partial fulfillment of the requirements for the degree of Doctor of Philosophy, The City University of New York

1991

This manuscript has been read and accepted for the Graduate Faculty in Physics in satisfaction of the dissertation requirement for the degree of Doctor of Philosophy.

4-15-91
Date

Carl Shakin
Chair of Examining Committee

4-17-91
Date

Joseph B. Kiegan
Executive officer

C. M. Shakin Carl Shakin

L.S. Celenza

M. K. Liou M. K. Liou

C. Trail

L. Cohen Leon Cohen

Supervisory Committee

The City University of New York

Abstract

THEORETICAL INTERPRETATION AND CALCULATION OF THE EUROPEAN MUON COLLABORATION EFFECT

By

Nanwei Cao

Advisor: Distinguished Professor Carl Shakin

First, we briefly review different models used in the description of deep inelastic scattering in nuclei (EMC effect). We discuss Fermi motion, nuclear binding, 'exess' pions in nuclei, Q^2-rescaling, etc. We present three novel calculations of the EMC effect which are of a 'microscopic' nature, in that the virtual photon is coupled to the quarks and quark wave functions are used. In our first analysis we investigated whether the EMC effect might be understood as having its origin in an off-mass-shell effect due to nuclear binding. Although we are able to fit the EMC data, we found that our results are very sensitive to the off-shell characterization of the struck quark. In our second

calculation, we use the analytic parameterization of the structure function, $F_2(x, Q^2)$, given by the EMC, in a convolution integral. In our discussion of Fermi motion and nuclear binding, we found that the results are not very satisfactory. We also considered the effect of 'swollen' nucleons in our analysis and found that our results improved somewhat. In our third approach to this problem, we considered the effect of final-state interactions (FSI). Instead of calculating FSI in detail, which is not really possible, we introduce a parameter δ representing the momentum lost by the struck quark due to FSI. Combining this analysis with our calculation of the effects of Fermi motion and binding, we find that our results are much improved.

Acknowledgements

To Professor Carl M. Shakin, my thesis advisor, I wish to express my deepest gratitude for his valuable guidance and constant encouragement throughout this thesis work. His help was important in bringing this work to completion.

I would also like to express my sincere gratitude to Professor Louis S. Celenza of Brooklyn College of the CUNY for the help given to me during the course of this work.

My thanks also go to Dr. Anthony Pantziris for the help given to me.

I wish to acknowledge with gratitude to Department of Physics of Brooklyn College and the Research foundation of the CUNY for the financial support during the course of this work, and the Brooklyn College Computer Center for allowing me to use their facilities.

TABLE OF CONTENTS

List of Tables

List of Figures

Chapter 1

Introduction

There are two fundamental reasons why lepton (μ or e) scattering is a powerful tool for studying nuclear structure. The first is that the basic interaction between the lepton and the target nucleus is well known. The lepton interacts with the electromagnetic charge and current density of the nucleus. Since the interaction is relatively weak, of order $\alpha = 1/137$, one can make measurements on the target nucleus without greatly disturbing its structure. With lepton scattering, one can immediately relate the cross section to the transition matrix elements of the local charge and current density operators and, thus, directly to the structure of the target itself. Of course, the same considerations apply to processes involving real photons, but leptons have the second great advantage that for a fixed energy loss ν of the lepton, one can vary the three-momentum transferred to the nucleus, $\vec{q}$, the only restriction being that the four momentum transfer should be space-like:

$$q^2 = \nu^2 - \vec{q}^2 < 0 .$$

In the case of real photons, for a given energy transfer, there is only a single

possible momentum transfer, $\vec{q}$, since the mass of a real photon is zero:

$$q^2 = \nu^2 - \vec{q}^2 = 0 .$$

Thus with leptons, we can study the complete $\vec{q}^2$ behavior of the transition matrix elements and map out the Fourier transforms of the transition charge and current densities. Therefore, one may determine the spatial distribution of the transition charge and current densities , and this is certainly a source of tremendously rich and unique information on the structure of nuclei.

Generally, the process of lepton scattering from a nucleus can be divided into four regions according to energy transfer ν, see Figure 1 :

1) Elastic scattering from the entire nucleus.
2) In the quasielastic region, at medium-energy transfer, the physics is well described by quasielastic scattering by individual nucleons.
3) At slightly higher energy, nucleon resonances are excited.
4) In the deep-inelastic region ($\nu > 1$ GeV), so much energy is deposited on a single quark that the nucleon breaks up in a complex manner.

In this work we will only consider the deep-inelastic scattering (DIS) process.

A typical deep-inelastic scattering process is illustrated in Fig. 2:

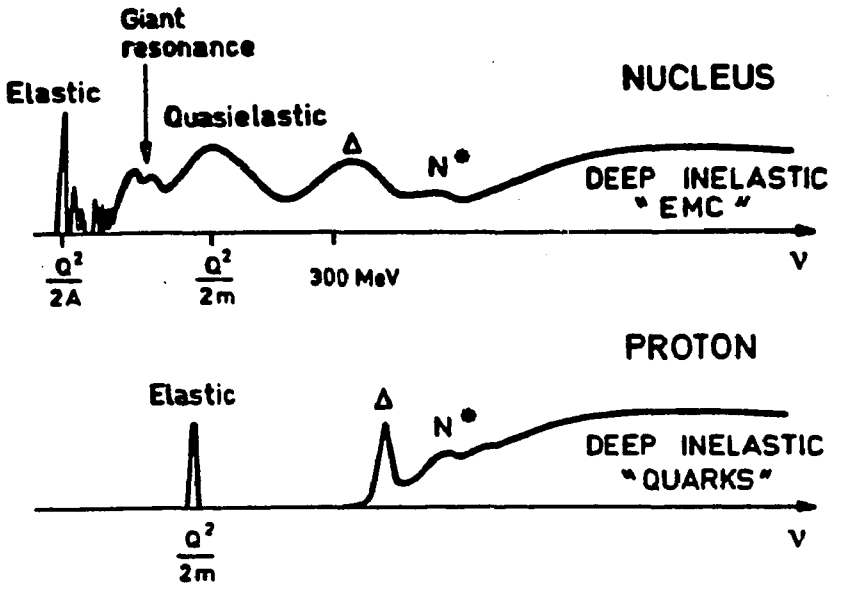

Figure 1. Schematic representation of the cross sections for lepton-nucleus and lepton-nucleon scattering as function of the energy transfer ν (for a fixed momentum transfer).

$$l + N \rightarrow l' + X \ ,$$

where l and l' are leptons, N is the nucleon and X is final hadronic state. Of particular interest to us is the region where the four-momentum transfer, $q^2 = (q^0)^2 - \vec{q}^2$, and the energy transfer, $\nu = q^0$, are large, e.g.,

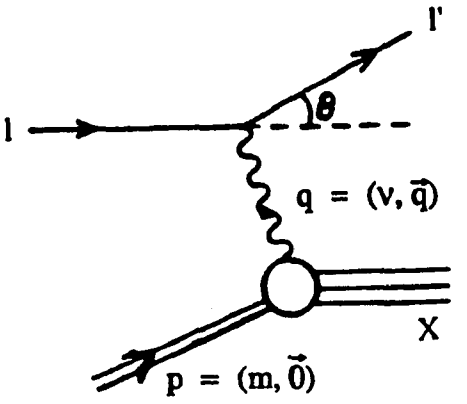

Figure 2. Illustration of a typical deep inelastic scattering process involving a nucleon at rest in the laboratory frame.

$Q^2 = -q^2 > 2\,GeV^2$ and $\nu > 1$ GeV. In this domain, the inclusive cross section can be related to structure functions which exhibit scaling. That is, to a first approximation, they depend only on the Bjorken variable $x = Q^2/(2P\cdot q) = Q^2/(2m\nu)$, rather than Q^2 and ν separately. Then,

$$\frac{d\sigma}{dxdy} = \frac{8\pi\,\alpha^2 mE}{Q^4} F_2(x, Q^2)\left[1 - y + \frac{y^2}{2(1+R(x,Q^2))}\right]. \qquad (1.1)$$

Here E is the energy of the incident lepton, $y = \nu/E$, and m is the nucleon

mass. Since a virtual photon is exchanged, both transverse and longitudinal cross sections are involved. $R(x,Q^2)$ measures the ratio of the inclusive cross sections for longitudinal and transverse photons: $R(x,Q^2) = \sigma_L(x,Q^2)/\sigma_T(x,Q^2)$. From experiment, it is found that R is small (< 0.1), weakly dependent on Q^2 and, if the target nucleon is replaced by a nucleus, essentially independent of atomic number.[1] The main information about the structure of the target is therefore contained in the structure function $F_2(x,Q^2)$ in the kinematic region considered here.

Before 1983, a standard expectation was that a nucleus behaves an incoherent collection of free nucleons in deep inelastic scattering. The cross section per nucleon for scattering on a nucleus was therefore expected to be the same for all nuclei, except for kinematic effects of the Fermi motion of the nucleons (i.e., the nucleons are not at rest, but move in orbits of some mean field). This implied that the quark momentum distribution in a nucleus was given simply by the appropriate average of the quark momentum distribution of the neutrons and protons in the nucleus. In 1983, the European Muon Collaboration[2] announced that the structure function (per nucleon) in iron differed significantly from that in deuterium. The ratio of the structure function of iron to deuterium $R_{EMC}(x,Q^2) = F_2^A(x,Q^2)/F_2^D(x,Q^2)$ differs from unity in a manner that cannot be attributed to Fermi motion of free nucleons. This result, known as the "EMC effect", was almost totally

unexpected because of the high momentum transfer involved (Q^2 up to 200 GeV^2). This observation has been confirmed in subsequent experiments, with various nuclear targets, by several groups.[3-7]

The EMC measured the cross section, and hence the structure function , for an iron nucleus. This structure function was divided by the mass number A to yield a structure function, which would be the same as that of a free nucleon, if iron consisted of 56 free nucleons at rest. Figure 3 shows the observed ratio of the structure functions (per nucleon) for iron and deuterium. A linear fit to the data points rose to ~ 1.15 at $x = 0$ and passed through zero at $x = 0.3$. (Corrections were made to take into account the difference of F_2^p and F_2^n for nuclei with $N > Z$.)

Because of the much greater intensity of their electron beam, a SLAC group[2] was very quickly able to check the EMC result for Fe. Their result for Fe confirmed the EMC effect for x between 0.3 and 0.7. At quite large x, they confirmed the theoretically expected rise above unity caused by Fermi motion. (There is no data in the large x region in the original EMC experiment.) A major surprise came at small x, however. They found no sign of an enhancement, which appeared to be a blow for a number of theoretical models.

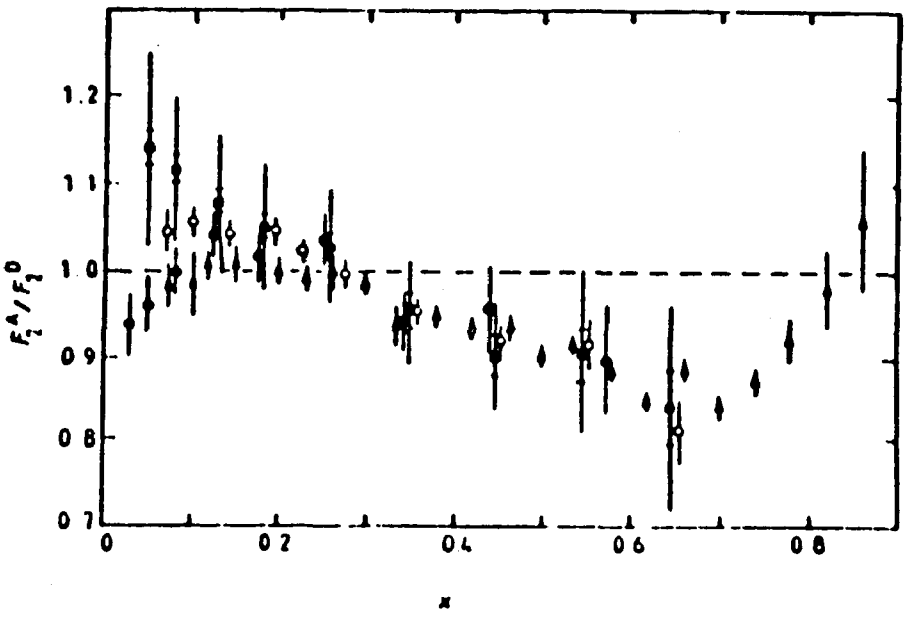

Figure 3. Some experimental data for the EMC effect. Full squares, EMC; open triangles, SLAC; full circles, Bodek et al; open circles, BCDMS.

Resurrected data from old SLAC experiments [2] and later work by BCDMS [4] tended to give results which lay between the SLAC and EMC results, indicating a definite but less dramatic enhancement below $x = 0.2$. Very recently this confusion appears to have been resolved. New SLAC data [1], new BCDMS data [7] and new EMC data [8], now appear to be consistent within their respective errors: The results can be described by dividing the x variation into

four regions:

1) very small x ($x < 0.05$, the so-called shadowing region). The Fe/D ratio drops below unity (see Fig. 4);
2) small x ($0.05 < x < 0.2$). There is a definite enhancement in the Fe/D ratio, but it is only of the order of 5%;
3) $0.2 < x < 0.7(0.8)$. The Fe/D ratio is below unity;
4) $x > 0.8$. The Fe/D ratio is greater than unity.

There is extra information potentially available from neutrino beams. For an isoscalar nucleon there are three new distributions which can be measured:

$$F_2^{(\nu,\bar{\nu})}(x, Q^2) = x(u + \bar{u} + d + \bar{d} + s + \bar{s}),$$

$$F_3(x, Q^2) = x(u - \bar{u} + d - \bar{d} + s - \bar{s}),$$

and

$$\bar{q}^{\nu} = x(\bar{u} + \bar{d} + 2\bar{s}),$$

where u, d, s are quark distribution functions. Results for these distributions are shown in Fig. 5. It is clear from Fig. 5 that the antiquarks are found mainly at x below 0.3 and the valence quarks dominate at large x. Indeed, a major reason for the excitement about the EMC effect concerned the large x behavior, because the (valence) quark structure of the nucleon appeared to be altered inside a nucleus. In addition, the enhancement at small x, where $q\bar{q}$ pairs dominate, suggested that there was an enhancement of the sea of a

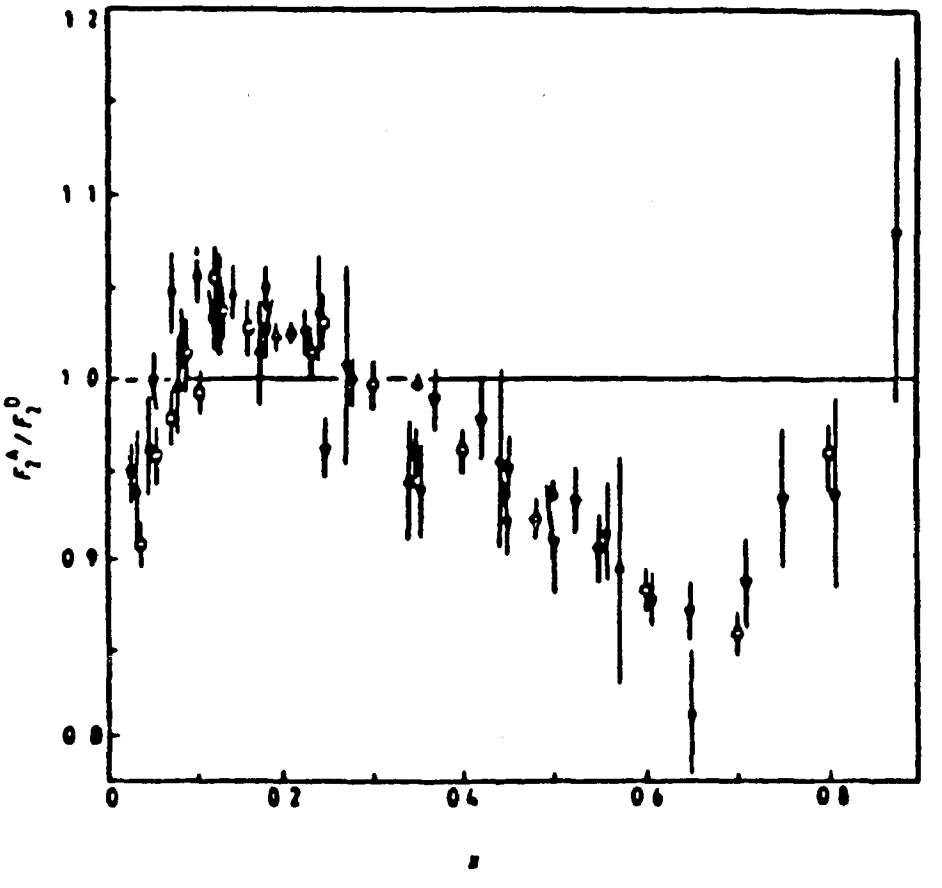

Figure 4. Summary of the most recent and reliable data for the ratio of the Fe (or Cu) and D structure functions. □, SLAC E61; ∇, SLAC E87; O, SLAC E139; Δ, SLAC E140; ●, BCDMS; ▲, EMC1; ▼, EMC2.

Figure 4

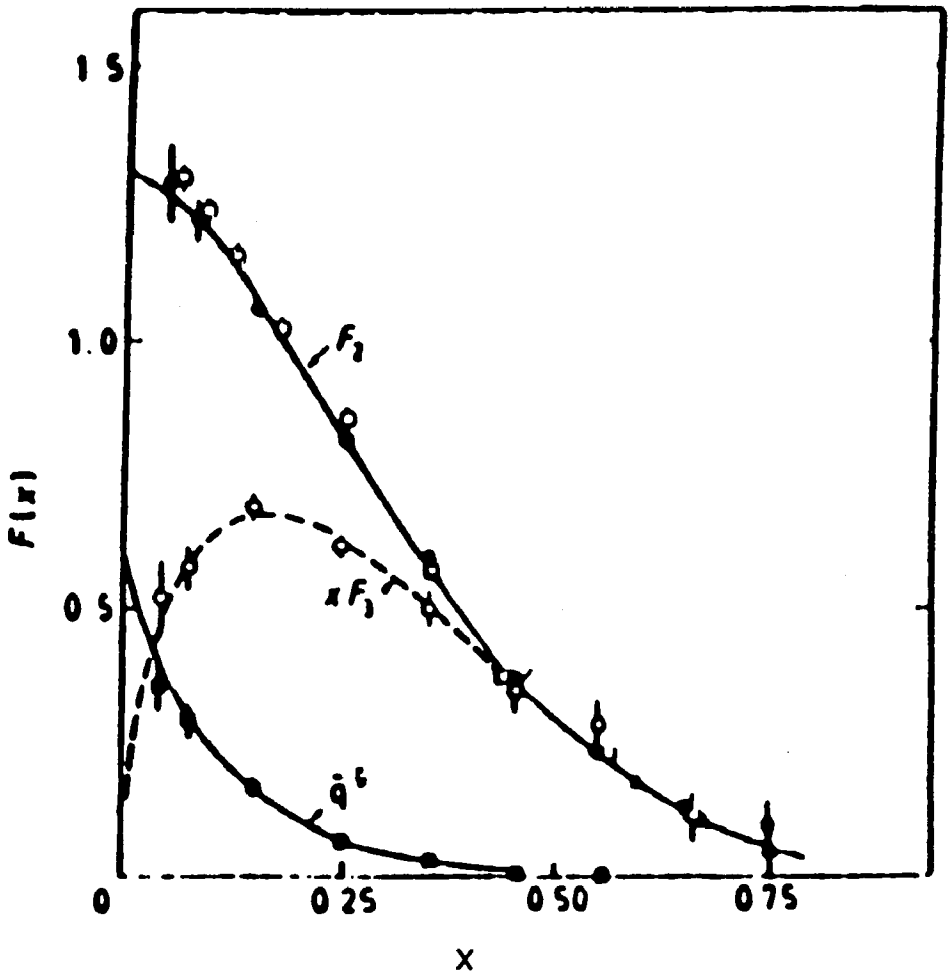

Figure 5. Summary of the experimental information on the DIS structure functions defined in the text (from Abramowicz et al., 1984). Here, $10 < Q^2 < 20$ GeV^2. ●,O, ■ : CDHS neutrino data. □ : $\frac{18}{5} F_2^{\mu N}$ (EMC muon data). Δ: $\frac{9}{5} F_2^{ed}$ (SLAC-MIT electron data

Figure 5

nucleon in nuclear matter.

Because the EMC effect was such a surprise, it has stimulated an enormous amount of theoretical work, and has led to some very exciting new ideas about nuclear structure. There are essentially two categories of theoretical models of the EMC effect which are presently considered as plausible. The first involves conventional nuclear physics, in which one must account for Fermi motion. However, Fermi motion is ultimately linked to nuclear binding in a finite nucleus. The introduction of nucleon binding leads to the introduction of off-mass-shell effects into the calculations. Finally, in conventional nuclear models the binding is associated with exchange of pions (and other heavier mesons). We should investigate the contribution to the EMC effect due to the presence of such mesons. A second category of explanation claims that the EMC effect is evidence for new QCD effects, such as a proposed change of the color confinement size of quarks within nuclei. (The interest in this effect is connected with the fundamental question of whether quarks and gluons play an important role in the description of nuclear forces.) This second category includes the Q^2-rescaling model, which is based on the observation that the EMC effect observed is similar to the violation of scaling behavior seen when structure functions are measured at various values of Q^2. Finally, we note that there are also models which deal with multi-quark clusters, which are assumed to be present in nuclei.

In the following, we present a brief introducton to these various models.

Chapter 2

Review of Models of the EMC Effect

2.1 Conventional Nuclear Physics Models of Deep Inelastic Scattering

2.1.1 Fermi Motion

From experiments of various groups, we can obtain values for σ^A/σ^D, or the ratio

$$R_{EMC}(x, Q^2) = F_2^A(x, Q^2)/F_2^D(x, Q^2) \ .$$

In order to avoid confusion with the quantity R defined in chapter 1, in the following, we use $R_{EMC}(x, Q^2)$ to represent EMC ratio. The existence of Fermi motion, i.e. the fact that nucleons move in their mean-field orbits, requires that calculations be made which relate the structure function of a nucleon to that of a nucleus. (These are often called 'Fermi smearing' calculations.)

In the rest frame of a free nucleon $P\cdot q = m\nu$ ($\nu = q^0$). However, if we consider a bound nucleon in the rest frame of a nucleus, $\vec{P} \neq 0$. Neither is $P^0 = m$, nor do we have $P^0 = \sqrt{\vec{P}^2 + m^2}$, because of nuclear binding. Since the 4-momentum of the struck nucleon is an unknown quantity, it is convenient to measure the structure functions in terms of $x = Q^2/(2m\nu) = x_A M_A/m$, where $x_A = Q^2/(2P_A\cdot q)$ is the scaling variable appropriate to the target nucleus (with $P_A\cdot q = M_A\nu$ in the target rest frame). The direct interpretation of x as the momentum fraction of quarks in the nucleon no longer holds when $P\cdot q \neq m\nu$. Thus, we need to account for Fermi motion and binding before comparing the nuclear structure function (per nucleon) with the free nucleon structure function.

From the theoretical point of view, DIS is entirely determined by a second-rank tensor $W^{\mu\nu}$. This is the Fourier transform of the commutator of two currents $j^\mu(y)$ and $j^\nu(0)$:

$$W_{\mu\nu}(P, q) = \frac{1}{2\pi} \bar{\sum_{pol}} \int d^4y\, e^{iq\cdot y} < N \,|[j^\mu(y), j^\nu(0)]|\, N > \,. \qquad (2.1)$$

In the laboratory frame, the momentum transfer q is usually chosen to be $(\nu, 0, 0, q_3)$. Also, $\overline{\Sigma}_{pol}$ denotes an average over target polarizations. (Alternatively we can put $\overline{\Sigma}_{pol} = \frac{1}{2}\Sigma_{pol}$, where Σ_{pol} denotes a sum over polarizations.)

On general grounds of Lorentz and gauge invariance for the electromagnetic interaction, the most general form of $W^{\mu\nu}$ is:

$$W^{\mu\nu} = \left(-g^{\mu\nu} + \frac{q^\mu q^\nu}{q^2}\right) W_1(\nu, Q^2) + \left(P^\mu - \frac{P\cdot q q^\mu}{q^2}\right)\left(P^\nu - \frac{P\cdot q q^\nu}{q^2}\right)\frac{W_2(\nu, Q^2)}{P^2} \quad (2.2)$$

(In rest frame $P^2 = m^2$.) W_1 and W_2 may be related to dimensionless structure functions, $F_1(x, Q^2)$ and $F_2(x, Q^2)$. Consider the diagram in Fig.6.

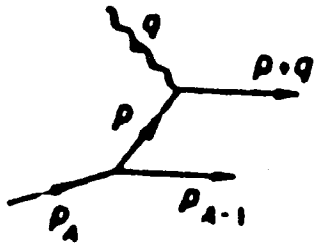

Figure 6. Kinematics for nuclear deep inelastic scattering where $P < P_F$.

We have,

$$P^0_{A-1} = (M^2_{A-1} + \vec{P}^2_{A-1})^{1/2} ,$$
$$\vec{P}_{A-1} = -\vec{P} ,$$
$$P^0 = P^0_A - P^0_{A-1} .$$

Here, all particles in the final state must be on their mass shell. The struck nucleon, with 4-momentum P, is off its mass shell, but its energy, P^0, is fixed in terms of its momentum $\vec{P}$ (and the energies of the other particles) by conservation of 4-momentum. In the target rest frame, $P^0_A = M_A$. Thus, P^0 is determined completely in terms of $|\vec{P}|$. (Here we have put the (A-1)-body residual system on shell. We will comment on that choice later in this work.)

We can write the tensor $W^A_{\mu\nu}$ for the target nucleus as an integral involving the response tensor for the off-shell nucleon constituents: [9]

$$W^A_{\mu\nu}(P_A, q) = \sum_{i=1}^{A} \int d^3P \left|\phi_i(\vec{P})\right|^2 W^N_{\mu\nu}(P, q) . \qquad (2.3)$$

Here $|\phi_i(\vec{P})|^2$ is the momentum distribution of a nucleon in its single-particle orbit, labeled i, and $\phi_i(\vec{P})$ is taken to be the nonrelativistic wavefunction of the nucleon in that orbit. Here we assume that an incoherent impulse approximation is valid. $W^A_{\mu\nu}$ must be of the form of Eq. (2.2) with m and P replaced by the mass and momentum of the target nucleus (i.e., M_A and P_A).

Lorentz scalars W_1^A and W_2^A may be defined as, (see Appendix A,)

$$W_1^A = -\frac{1}{2}\left(g^{\mu\nu} - \frac{\hat{P}_A^\mu \hat{P}_A^\nu}{\hat{P}_A^2} \right) W^A_{\mu\nu} \ , \tag{2.4}$$

and

$$W_2^A = -\frac{1}{2}\frac{M_A^2}{\hat{P}_A^2}\left(g^{\mu\nu} - \frac{3\,\hat{P}_A^\mu \hat{P}_A^\nu}{\hat{P}_A^2} \right) W^A_{\mu\nu} \ , \tag{2.5}$$

where $\hat{P}_A^\mu = P_A^\mu - (P_A \cdot q)q^\mu/q^2$.

Assuming an expansion for $W^A_{\mu\nu}(P_A, q)$ analogous to Eq. (2.2), we then

obtain (in the target rest frame): (see Appendix B)

$$W_1^A = \sum_i \int d^3p \left|\phi_i(\vec{p})\right|^2 \left[W_1^N + W_2^N \frac{p_\perp^2}{2P^2}\right] , \tag{2.6}$$

$$W_2^A = \sum_i \int d^3p \left|\phi_i(\vec{p})\right|^2 \left(\left[\frac{(p^0q^3 - p^3q^0)}{q^3}\right]^2 + \frac{p_\perp^2}{2}\left[\frac{Q^2}{(q^3)^2}\right]\right)\frac{W_2^N}{P^2} . \tag{2.7}$$

We note that Eq. (2.2) holds for a free target, because P_μ^A and q_μ are the only 4-vectors available from which we may construct a non-trivial tensor $W_{\mu\nu}^A$. However, this is no longer the case for an interacting (or off-shell) particle. For example, suppose that the nucleons interact via a vector potential A_μ , such as might arise from ω meson exchange. How is one to incorporate this into $W_{\mu\nu}^N$? This problem of specifying off-shell behavior is intrinsic to this approach, and appears also in other attempts to derive a convolution formula. [10,11] The most common way around this difficulty is to ignore it. One is left with the further problem of identifying the off-shell structure functions, W_1^N and W_2^N, in Eq. (2.6) and Eq. (2.7). These structure functions depend on the Lorentz invariants P^2, $P\cdot q$ and q^2 (or Q^2). For a

free target, P^2 is fixed ($= m^2$), and therefore irrelevant. However, in the off-mass-shell case, W_1^N and W_2^N may possess a P^2 dependence. Bodek and Ritchie [12] and most authors take these structure functions to be the same as those for an on-shell nucleon at the same Q^2 and final-state invariant mass $W^2 = (P+q)^2$. This is not an obvious choice. Dunne and Thomas [13, 18] have discussed the behavior of the off-mass-shell nucleon structure function, and have argued for a shifted value of Q^2. Their model is then mathematically identical to a rescaling model which we will discuss later, but has a quite different interpretation. Their change of scale is a change of the mass and not a change of the confinement scale.

In chapter 3, we will present calculations which are of a more 'microscopic' nature, in that the virtual photon is coupled to the quarks in our model and quark wave functions are used in the calculations. We use an expression for $W_{\mu\nu}$ given in terms of Lorentz-invariant quantities, which are off-mass-shell generalizations of $W_1(x, Q^2)$ and $W_2(x, Q^2)$. The introduction of nucleon binding requires that we make an off-mass-shell extrapolation of W_1 and W_2, within the context of our dynamical model.

In the scaling region, and assuming the Bjorken limit, the

convolution formulas, Eq. (2.6) and Eq. (2.7) reduce to

$$F_1^A(x) = \sum_i \int_x^{\frac{M_A}{m}} \frac{dy}{y} f_i(y) F_1^N(\tfrac{x}{y}) \ , \tag{2.8}$$

$$F_2^A(x) = \sum_i \int_x^{\frac{M_A}{m}} dy\, f_i(y) F_2^N(\tfrac{x}{y}) \ , \tag{2.9}$$

where

$$f_i(y) = \int d^3P\, y\, \delta(y - \frac{P^0 + P^3}{m}) \left|\phi_i(\vec{P})\right|^2 . \tag{2.10}$$

We have used

$$F_1^A(x) \equiv mW_1^A(P_A, q) \ , \tag{2.11}$$

$$F_1^N(x) \equiv mW_1^N(P, q) \ , \tag{2.12}$$

$$F_2^A(x) \equiv \frac{P_A \cdot q}{M_A} W_2^A(P_A, q) \xrightarrow[B_j]{} \nu W_2^A \ , \tag{2.13}$$

$$F_2^N(x) \equiv \frac{P \cdot q}{m} W_2^N(P, q) \xrightarrow[B_j]{} y\nu W_2^N \ . \tag{2.14}$$

There is some controversy as to whether a 'flux factor' [(i.e. the factor y in Eq. (2.10)] should be included. If we had ignored the factor of y in Eq. (2.10), the average distribution for a Fermi gas would be

$$f(y) = \frac{\gamma}{\rho} \int \frac{d^3P}{(2\pi)^3} n_P\, \delta(y - \frac{P^0 + P^3}{m}) \ . \tag{2.15}$$

Frankfurt and Strikman [14] have emphasized the presence of the y factor. They have argued that its inclusion, without any renormalization of the

wavefunction, leads to a violation of the sum rule

$$\int_0^{\frac{MA}{m}} dy\, f(y) = 1 \,.$$

It is suggested that one should use

$$\int d^3P \left(\frac{P^0 + P^3}{P^0}\right) \left|\phi_i(\vec{P})\right|^2 \theta(P^0 + P^3) = 1 \qquad (2.16)$$

as the normalization condition.

This question has been investigated by Jung and Miller [11] and Bickerstaff [15], who examined a Fermi gas in the Bjorken limit using a correlation function approach. They found that, in the absence of interactions, the factor of y neglected in the transition from Eq. (2.10) to Eq. (2.15) was actually a factor $(m/P^0)y = 1 + P^3/P^0$. Thus for a free Fermi gas one has

$$f(y) = \frac{\gamma}{\rho} \int \frac{d^3P}{(2\pi)^3} n_P \left(1 + \frac{P^3}{P^0}\right) \delta\left(y - \frac{P^0 + P^3}{m}\right) . \qquad (2.17)$$

Note that, in the evaluation of $\int dy\, f(y)$, the term involving P^3 averages to zero, so that the correct sum rule for f(y) of Eq. (2.17) is retained. Using Eq. (2.17), $\langle y \rangle = \langle P^0/m \rangle + \frac{1}{3} \langle \vec{P}^2/(mP^0) \rangle$. Thus, the effect of

Fermi smearing is modified. (Without the flux factor y, we have $< y > = < P^0 > / m > 1$.) Thus, $(1/A)\, F_2^A/F_2^N$ will be enhanced by the additional term, $1/3 < \vec{P}^2 > / (mP^0)$. The inclusion of such a factor reduces the size of the effect.

Clearly, a calculation of only the dynamics associated with Fermi motion cannot explain the EMC effect.

2.1.2 Nuclear Binding

The nuclear binding model of the EMC effect was developed independently by Akulinichev et al. [16] and Dunne and Thomas [13]. Their model shares the basic principles of the incoherent impulse approximation used in the earlier work of Atwood and West [17] and Bodek and Ritchie [12] dealing with Fermi motion. The key difference is in the treatment of the energy of recoil of the A-1 nucleus. Bodek and Ricthie asserted that the residual (spectator) nucleus was not in a highly excited state. On the contrary, Akulinichev et al. and Dunne and Thomas recognized that it is, in fact, left in a highly excited hole state $(A\text{-}1)_i$, where i is the state in which the struck

nucleon lay. The separation energy, ε_i, of a nucleon in orbital i is defined by

$$\varepsilon_i = M_A - M^i_{(A-1)} - m \ . \tag{2.18}$$

Thus the energy of the struck nucleon becomes

$$P^0 = m + \varepsilon_i - T_R \ , \tag{2.19}$$

where $T_R = \vec{P}^2/2M^i_{A-1}$ is the recoil kinetic energy of the (A-1)-body nucleus. The recoil correction, T_R, is important for a light nucleus such as deuterium [12, 13, 18], but may be neglected for medium and heavy nuclei. (Akulinichev et al. sometimes omitted T_R in deuterium, a point criticized by Dunne and Thomas.) However, the main difference between various calculations rests with the value used for ε_i. First, however, let us understand the role of this quantity in the calculation.

The binding-energy model provides an expression for P^0 which is to be used in calculating a distribution, f(y), in a convolution formula. When we discussed Fermi motion, we saw that the effect of the smearing integral was controlled to a large extent by the expectation value of y. ($\langle y \rangle = \langle P^0 \rangle /m$.) We expand $F_2(x/\langle y \rangle)$ in a Taylor series about $x/\langle y \rangle$. For $x \leq 0.75$, if the distribution f(y) is very narrow about $\langle y \rangle$, we obtain

$$F_2^A(x)/A \approx F_2^N(x/\langle y\rangle) \ . \qquad (2.20)$$

In the case of pure Fermi motion, we saw that $\langle y\rangle$ was a number greater than unity, because of the (positive) kinetic energy contribution to P^0. The essential feature of the binding model is the observation that, because the nucleon is bound, there must be an attractive potential, such that the sum of the potential, and kinetic energy is negative. Therefore, $\langle y\rangle < 1$. Hence, because F_2 is a decreasing function of x, we see from Eq. (2.20) that, whereas pure Fermi motion leads to $(1/A)F_2^A(x)/F_2^N(x) > 1$, the inclusion of binding changes the Fermi smearing prediction so as to yields a ratio less than unity (in the region $x < 0.75$). For x near 1, the binding effect is swamped by the enhancement arising from the cutoff imposed on f(y) via the convolution integration. Thus, the qualitative features of the EMC ratio at medium and large x are reproduced. Actually, the combined effect of binding and Fermi motion is to induce an approximate x-rescaling, $x \rightarrow x/\langle y\rangle$, in the constituent nucleon structure functions.

There is a question as to the appropriate value of $\langle \varepsilon_i \rangle$ to be used, where $\langle \varepsilon_i \rangle$ is the average single-particle energy of a nucleon in a

nucleus. Dunne and Thomas [13] used $< \varepsilon_i > = -26$ MeV, smaller than the -39 MeV advocated by Akulinichev et al., who claimed that they could explain the EMC effect. Dunne and Thomas failed to get sufficient depletion. If one uses measured separation energies, within the naive single-particle model, the discrepancy becomes worse for heavier nuclei, because $< \varepsilon_i >$ saturates, whereas the EMC depletion increases with an increase in the nuclear density. As we mentioned before, Dunne and Thomas [13, 18] proposed making up the difference with an off-mass-shell effect.

It is important to use the 'right numbers'. Li et al.[21] present calculations of the binding effect in a Hartree-Fock model using a density-dependent Skyrme force. They obtain $< \varepsilon_i > = -26$ MeV in Fe, and, therefore, their results are very similar to those of Dunne and Thomas [13].

Consider a model based upon the use of binding energies. If we use a Lorentz-invariant spectral function, $S(P) = (2\pi)^{-3} \sum (m/P^0) |\phi_i(P)|^2 \delta(P^0 - m - \varepsilon_i)$, we obtain an extra factor $(m/P^0)y = (1 + P^3/P^0)$ in f(y), which agrees with the free Fermi-gas result of Bickerstaff [15] and Jung and Miller [11]. Including this factor means that the effect of the separation energy is reduced by about

+15 MeV. If we use $<\varepsilon_i>$ = -39 MeV, one finds a 40% reduction in the predicted depletion. If we use $<\varepsilon_i>$ = -26 MeV, the factor $(1 + P^3/P^0)$ wipes out 60% of the depletion.

Although the binding model is in trouble, it may play an important role in the correct treatment of Fermi motion. Of course, there is some question as to whether the entire calculational procedure is correct.

2.1.3 Pion-exchange Model

The qualitative features of the EMC effect at intermediate and large values of x may be understood by including binding corrections and Fermi motion. However, it was clear that this success came at a price: the bound nucleons did not carry all of the momentum of the nucleus —the deficiency being of order ε/m. Since nuclear binding is conventionally regarded as the result of the exchange of virtual mesons between nucleons, it is natural to propose that the missing momentum is carried by these mesons. Compared to a nucleon in free space, one may expect an increase in the number of virtual pions per

nucleon in a nucleus. This increase is thought to imply an increase in the number of sea quarks and might explain the rise at small x in the EMC ratio. Because the "excess" pions in a nucleus carry some of the momentum of the nucleus, as a consequence of overall momentum conservation, the nucleons do not carry all of the momentum of the nucleus. Hence, the valence quarks in the nuclear target carry a smaller fraction of the total momentum than in a free nucleon. In order to balance momentum, Llewellyn-Smith [22] proposed a purely phenomenological shift in the Fermi motion correction, which is a form of x-rescaling. Llewellyn-Smith, Ericson and Thomas [23] (LET) make the calculation in the frame where the initial nucleus is at rest, using standard quantum mechanics and covariant field theory. In this theory, four-momentum is conserved at the πNN vertex. Because the recoiling nucleon occurs in the final state, it must be on-mass-shell and thus the pion is forced to be off-shell and has negative energy:

$$k^0 = m - \sqrt{m^2 + \vec{k}^2} ,$$

where $\vec{k}$ is the pion momentum.

On the other hand, Berger and Coester (BC) [24-26] carry out all their formal work using Dirac's light-front dynamics. In this theory, the evolution of a system is described, not in terms of usual time variable, but by $x^+ =$

$x^0 + x^3$. The component P^- of momentum is not conserved at vertices and consequently it is possible to have both the recoiling nucleon and the pion on-mass-shell, i.e.

$$k^0 = +\sqrt{m_\pi^2 + \vec{k}^2} \ .$$

However, the Berger-Coester distribution, $f_\pi^{BC}(y) = \int d^3k \, \rho(k) \, \delta(y - \frac{k^0 + k^3}{m_\pi})$,

results from a mixture of time-ordered perturbation theory and light-front dynamics. Because energy, and hence k^+, is not conserved in the former we are not able to interpret the calculated $f^{BC}(y)$ as a distribution of momentum fraction y, as required for insertion in the convolution formula. The difference between the approximations made by LET and BC leads to different results. (The experimental work of Carey et al. [27] neither supports nor contradicts the hypothesis that 'enhanced' nuclear pions can explain the small-x enhancement of the EMC effect. However, recent studies of the Drell-Yan process yield no such enhancement and are considered to be a blow against the model of "excess mesons".)

The 'conventional nuclear physics' approach (describing Fermi motion,

nuclear binding, pion-exchange), when used to understand the EMC effect, can fit the present data within the limits of our knowledge of nuclear structure. There are various unresolved questions– namely, the possible importance of off-shell effects and the possible failure of the convolution hypothesis, as mentioned above.

2.2 Novel QCD Effects

2.2.1 Dynamical Rescaling Model

At moderate values of Q^2, say greater than 2 GeV^2, the structure functions depend on Q^2 only through $\ln Q^2$ (leading twist) and this implies a slow variation. (Higher twist contributions lead to power-law corrections in Q^2.) This variation with $\ln Q^2$ is calculable in perturbative QCD. Since, in QCD, the target dependence should reside in non-perturbative (unknown) matrix elements, it was extremely surprising to discover that the EMC data on Fe and D could be related over a wide range of x ($0.2 < x < 0.7$) by a simple shift in momentum scale:

$$F_2^{Fe}(x, Q^2) = F_2^D(x, \xi Q^2) . \tag{2.21}$$

The parameter ξ must depend on Q^2, but for $Q^2 \sim (5 - 10)\,GeV^2$, which is typical of the EMC data, ξ was found to be about 2.

Both Nachtman and Pirner [28] and Close et al. [29] interpreted this rescaling as resulting from increasing deconfinement of the quarks in heavier nuclei. The work of Close et al. had its theoretical foundation in an idea about the relationship between quark models and parton distributions. The idea is that a quark model (and most are valence-quark dominated) should represent the structure of a nucleon as seen with poor momentum resolution, that is, at low Q^2. They have proposed that there may exist some momentum scale, $Q^2 = \mu_0^2$, at which the quark model could be used to calculate the twist-two valence-quark distribution. Close et al.[29, 30] and Jaffe et al.[31] took $\mu_0^2 = 0.66\,GeV^2$. They proposed that this scale was target dependent, i.e. that the valence distributions in a nucleus and in free space might obey

$$q_V^A(x, \mu^2) = q_V^N(x, \mu_0^2) . \tag{2.22}$$

Using leading-order QCD, one finds the corresponding distributions at the

same higher Q^2:

$$q_{V}^{A}(x, Q^2) = q_{V}^{N}(x, \xi(Q^2)Q^2) \ , \tag{2.23}$$

where

$$\xi(Q^2) = (\mu_0^2/\mu^2)^{\alpha(\mu^2)/\alpha(Q^2)} \ . \tag{2.24}$$

This model, which relates a target-dependent scale change for quarks to a shift in Q^2, is known as a dynamical rescaling model. This scale change was interpreted using results of a calculation of bag-model structure functions. Jaffe [32] obtained a relationship between the quark distributions in two bags of different radii, R_0 and R. Because the simplest bag model has only one scale (its radius), Close et al. [29] proposed

$$R^2/R_0^2 = \mu_0^2/\mu^2 \ . \tag{2.25}$$

That is, a bound nucleon might have a radius, R, which is larger than R_0, the radius of a free nucleon.

The deficiencies of this model are: First, a large increase in nucleon size (in Fe, it was found to be about (10-20)%) does seem rather unlikely [33, 34]. Second, the dynamical rescaling model cannot explain the rise in the EMC ratio above unity ($R_{EMC} > 1$) at large x.

2.2.2 Multi-quark Clusters

The Drell-Yan-West rule relates the behavior of the quark momentum distributions $q_i(x)$ to the number of quarks in the target, say N. When the struck quark does not suffer spin-flip it predicts

$$q_i(X) \underset{X\to 1}{\to} (1 - X)^{2N-3} \qquad X \approx x/A \ . \tag{2.26}$$

Spin-flip costs another power of (1-X). Krzywicki [35] proposed that the nucleus should be taken to be a collection of 3A valence quarks plus 'pions' and gluons. The valence quark distributions in nucleons behaved like $(1-x)^3$, while meson and gluon distributions behaved like $(1-x)^5$, for $x \sim 1$. Having fixed the parameters of the model, one can predict the nuclear momentum distributions. For example, for pion and gluons one finds $(1-X)^{5A}$. With A large, this approximates e^{-5X}, which does not drop as fast as $(1 - x)^5$ (as $x \to 1$). Thus, Krzywicki predicted an enhancement in the number of 'hard' (large momentum in the DIS sense) pions and gluons in the nucleus. As a consequence, one might expect the valence quark distribution to be softened, i.e., to lose momentum. This prediction is at least quantitatively consistent with the EMC effect. From Krzywicki's work,

we see that any non-nucleonic component in the nucleus may lead to a different quark momentum distribution. Many authors have pursued this idea, with clusters of 6, 9 or 12 quarks replacing nucleons at some level of probability. Jaffe [10] and Hoodbhoy [36] suggest that antisymmetrisation forces one to deal explicitly with quark degrees of freedom in the short-range part of the nucleon-nucleon wavefunction.

The model of the nucleus as a giant quark bag is objectionable, since we have a successful traditional picture of the nucleus as a collection of bound nucleons. It seems unimaginable that one could reproduce the successes of this useful picture by replacing it with a single bag of quarks and gluons.

Chapter 3

Alternative Theoretical Interpretations and Calculational Procedures

We present three novel calculations of the EMC effect. In our first analysis we paid particular attention to the off-mass-shell characterization and transformation properties of the response tensor $W_{\mu\nu}$. We thought that the EMC effect might be understood as having its origin in an off-mass-shell effect due to nuclear binding. However, our calculation is different from those studies of binding effects which make use of the convolution formulas of the parton model. (It is also different from the study of Dunne and Thomas [13, 18], who consider off-mass-shell effects as introducing a Q^2 rescaling. Their parameter, $\xi = (m^2/P^2)^{\alpha_s(P_A^2)/\alpha_s(Q^2)}$, has a completely different interpretation than the parameter ξ of the dynamical rescaling model.)

Although we are able to fit the EMC data, we found that our results are very sensitive to the off-shell characterization of the struck quark.

In our second calculation, we use the analytic parametrization of the structure function, $F_2^p(x, Q^2)$, given by EMC [37], in a convolution integral. In this case, the results are not very satisfactory, since the EMC ratio is too large for small x in this calculation. Thus far, we have discussed Fermi motion and binding. We also considered the effect of 'swollen' nucleons in our analysis. We found that our results improved somewhat.

In our third approach to this problem, we considered the effect of final-state interactions (FSI). this feature has been neglected by all other authors. Instead of calculating the FSI in detail, which is not really possible, we introduce a parameter δ, representing the momentum lost by the struck quark due to the FSI. Combining this analysis with the Fermi motion and binding, our results seem to be much improved. (In Sec. 3.4 we will discuss another approach to FSI due to Glazek and Shakin.)

3.1 Off-Mass-Shell Dynamics in a Microscopic Calculation of the EMC

Our calculations are of a more 'microscopic' nature, in that the virtual

photon is coupled to the quarks in our model and quark wave functions are used in the calculations. Further, we are able to present a more transparent treatment of various kinematic aspects of the calculation, since we use an expression for $W_{\mu\nu}$ given in terms of Lorentz-invariant quantities, which are off-mass-shell generalizations of $W_1(x, Q^2)$ and $W_2(x, Q^2)$. (We note that $W_{\mu\nu}$ is usually defined for on-mass-shell nucleons; the introduction of nucleon binding requires that we make an off-mass-shell extrapolation of that quantity.) As we will see, our analysis requires the choice of two parameters, one of which determines the momentum content of the quark wave functions used, while the other is an oscillator parameter of a (translationally invariant) nuclear shell model. The nuclear size parameter, b, is fixed by fitting the electromagnetic form factors of nuclei, such as ^{4}He, ^{12}C and ^{40}Ca. The mass parameter μ, which determines the form of the (valence) quark wave functions, is fixed by fitting experimental data for $F_2^p(x)$, the structure function of the proton, using our model of nucleon structure.

In Section 3.1.1, we review the calculation of the structure function of an isolated nucleon in terms of quark wave functions[38, 39]. In Section 3.1.2, we present an expression for the (averaged) structure function of a nucleon in finite nuclei. There, we present the results of our numerical calculations of the EMC

effect in finite nuclei. Section 3.1.3 is devoted to the discussion of the quark 'sea', while Section 3.1.4 contains some conclusions and discussion.

3.1.1 Calculation of Nucleon Structure Functions in Vacuum

In the following discussion, we will use the notation of Ref.38 (see Fig. 7). Here, P denotes the four-momentum of the nucleon. The authors of Ref. 38 calculated the structure functions, $W_1(x,Q^2)$ and $W_2(x,Q^2)$, for a nucleon at rest. Since W_1 and W_2 are Lorentz scalars, we can obtain their values for on-mass-shell nucleons in motion by making the substitution $\nu \rightarrow (P.q)/m$. In the present work, we generalize this calculation to describe nucleons of finite velocity, which are off-mass-shell ($P^2 \neq m^2$) due to nuclear binding.

As we mentioned before, binding effects are usually discussed within the context of a convolution formula which involves the calculation of an average over the free-space nucleon structure function[40]. The introduction of binding effects then leads to a formula in which the free structure function is evaluated at a shifted values of the Bjorken variable x. It is our belief that a proper calculation of the effect of binding is significantly more complicated than

those to be found in the literature. For example, we consider the symmetric part of the response tensor of a nucleon. (In this work, we discuss spin-averaged scattering. Therefore, we need only consider the symmetric part of $W_{\mu\nu}$.) We have,

$$W_{\mu\nu}(P, q) = W_1(x, Q^2)\left(-g_{\mu\nu} + \frac{q_\mu q_\nu}{q^2}\right) + W_2(x, Q^2)\frac{\hat{P}_\mu \hat{P}_\nu}{P^2}, \tag{3.1}$$

where

$$\hat{P}_\mu = P_\mu - (P\cdot q)q_\mu/q^2, \tag{3.2}$$

etc. Here $x = Q^2/(2P\cdot q)$. In free space, one usually suppressed reference to the dependence on P^2, since $P^2 = m^2$. However, binding effects lead to $P^2 \neq m^2$ in a nuclear environment. Therefore, to study such effects one should properly consider structure functions which are functions of three variables:

$$W_{\mu\nu}(P, q) = W_1(P^2, x, Q^2)\left(-g_{\mu\nu} + \frac{q_\mu q_\nu}{q^2}\right) + W_2(P^2, x, Q^2)\frac{\hat{P}_\mu \hat{P}_\nu}{p^2}. \tag{3.3}$$

Equation (3.3) may be taken as a definition of our extrapolation of the response tensor $W_{\mu\nu}(P, q)$ for the off-mass-shell case, $P^2 \neq m^2$. It should be clear that there is no way to insert the dependence on the variable P into the

convolution formulas of the parton model, which involve only free-space structure functions. [40]

In order to calculate the off-mass-shell response tensor of Eq. (3.3), one needs a microscopic model. As noted above, we will make use of the model introduced in Ref. 38 . The characteristics of the model may be seen in Fig .7 , where the target is a nucleon composed of a quark of momentum P - K and a residual system of momentum K. In order to calculate a cross section, the residual system is placed on mass shell, $K^0 = (\vec{K}^2 + m_d^2)^{1/2}$, with $m_d = \sqrt{P^2}$. (When $P^2 = m^2$, $m_d = m$.) The quark has momentum $p = P - K + q$ after absorbing the virtual photon and is also placed on mass shell, $p^2 = 0$. (One does not attempt to describe hadronizaton in a model of this type.)

In order to describe the EMC effect, we evaluate the diagram shown in Fig. 8 . (This is equivalent to the calculation of the imaginary part of the virtual Compton amplitude represented in Fig. 8 .) We can calculate $W_{\mu\nu}(P, q)$ from the knowledge of matrix elements of the electromagnetic current [38]

$$W^{\mu\nu}(P, q) = (2\pi)^6 \sum_{P_X} < \vec{P}, s, t | J^{\mu}(0) | \vec{P} >< \vec{P}_x | J^{\nu}(0) | \vec{P}_x, s, t > \delta (P^0 - P_x^0 - q^0)$$

(3.4)

where J^μ is expressed in terms of quark fields,

$$J^\mu(0) = \bar{q}(0)\,\gamma^\mu\,(\frac{1}{6} + \frac{\tau_3^q}{2})\,q(0)\,. \tag{3.5}$$

The final state may be specified as in Fig. 7, so that

$$< \vec{P}_x |\ J^\mu(0)\ | \vec{P}, s, t > = < \vec{p}, s_q\, t_q; -\vec{K}, S M_S T M_T a |\ J^\mu(0)\ | \vec{P}, s, t >\,, \tag{3.6}$$

where p, s_q and t_q are quark momentum, spin and isospin variables. The other variables refer to the residual system.[38] After taking the average over the nucleon spin projection s, we found [38] for the case of zero quark mass,

$$W_{\mu\nu}(P, q) = \frac{1}{2}\,\mathrm{Tr}\int \frac{d\vec{K}}{2E_q(P)}\,\gamma_\mu \not{P}\,\gamma_\nu\,\delta(\,p^0 + E_d(\vec{K}) - \nu - P^0\,)\left[\frac{1}{6} + \frac{\tau_3^q}{2}\right]^2 (2\pi)^3$$

$$\times \sum_{S\,M_S\,T\,M_T} \left[\frac{1 + (-1)^{S+T}}{2}\right] < -\vec{K}, S\,M_S\,T\,M_T\,a \,|\, q_a(0) \,|\, \vec{P}, s\,t > \tag{3.7}$$

$$\times\ < \vec{P}, s\,t \,|\, \bar{q}_a(0) \,|\, -\vec{K}, S\,M_S\,T\,M_T\ a\ > .$$

Here $p^0 = |\,\mathbf{P} + \mathbf{K} + \mathbf{q}\,|$, since the quark is on mass shell. For convenience, we perform the calculation in the rest frame of the nucleon ($\vec{P} = 0$, $P^0 = m$).

In that frame, we can define a quark wave function $\psi^{(s_q)}(\vec{K})$

$$<-\vec{K}, S\,M_S\,T\,M_T\;\; a \mid q_{\alpha\rho a}(0) \mid \vec{P} = 0, s\;t>$$

$$= \sum C^{T}_{M_T\, t_q\, t} \sum C^{S}_{M_S\, s_q\, s} \frac{\delta_{a\bar{a}}}{\sqrt{2}} \psi^{(s_q)}_{\alpha}(\vec{K})\, \chi^{(t_q)}_{\rho} \quad . \tag{3.8}$$

We use the form

$$\psi^{(s_q)}(\vec{K}) = \frac{1}{\sqrt{4\pi}} \begin{bmatrix} R_u(\vec{K})\, \chi^{(s_q)}_{\rho} \\ \vec{\sigma}\cdot\hat{K}\, R_l(\vec{K})\, \chi^{(s_q)}_{\rho} \end{bmatrix} . \tag{3.9}$$

The wave function is taken to be independent of P^0. This approximation is justified by the fact that, in a nucleus, the deviation from the free case is small, $P^2 \approx m^2$. Using the formalism of Ref. 38, we find

$$W^{\mu\nu}(P, q) = \frac{2\pi}{|\vec{q}|} \int_{K_1}^{K_2} d|\vec{K}|\,|\vec{K}| \left((m_q A - p\cdot B) \left[g^{\mu\nu} - \frac{q^{\mu}q^{\nu}}{q^2} \right] + \hat{P}^{\mu}\hat{B}^{\nu} + \hat{P}^{\nu}\hat{B}^{\mu} \right) ,$$

(3.10)

where the quantities $A(\vec{K})$ and $B_{\mu}(\vec{K})$ were used to parameterize the valence quark density matrix. We had [38]

$$A(\vec{K}) = \frac{1}{8\pi}\left[R_u^2(\vec{K}) - R_l^2(\vec{K}) \right] , \tag{3.11}$$

$$B^0(\vec{K}) = \frac{1}{8\pi}\left[R_u^2(\vec{K}) + R_l^2(\vec{K}) \right] , \tag{3.12}$$

$$\vec{B}(\vec{K}) = \frac{\hat{K}}{4\pi} R_u(\vec{K})\, R_l(\vec{K}) . \tag{3.13}$$

The limits of the $|\vec{K}|$ integral in Eq. (3.10) were found to be

$$K_1 = | \alpha - \beta | \tag{3.14}$$

and

$$K_2 = \alpha + \beta , \tag{3.15}$$

where

$$\alpha = \frac{\nu + P^0}{2}\left(\left[1 - \frac{(m_d + m_q)^2}{W^2} \right] \left[1 - \frac{(m_d - m_q)^2}{W^2} \right] \right)^{1/2} , \tag{3.16}$$

$$\beta = \frac{|\vec{q}|}{2}\left(1 + \frac{m_d^2 - m_q^2}{W^2} \right) , \tag{3.17}$$

with

$$W^2 = (\nu + P^0)^2 - |\vec{q}|^2 . \tag{3.18}$$

Here, we take $m_q = 0$ and $m_d = \sqrt{P^2} = m$ for a nucleon in vacuum.

Using Eq. (3.10), we form the invariants

$$I_1 = W^{\mu\nu}\hat{P}_\mu\hat{P}_\nu \ , \tag{3.19}$$

$$= - W_1\hat{P}^2 + W_2\hat{P}^4/m^2 \ , \tag{3.20}$$

and

$$I_2 = W^\mu{}_\mu \ , \tag{3.21}$$

$$= -3W_1 + W_2\hat{P}^2/m^2 \ . \tag{3.22}$$

Since I_1 and I_2 are Lorentz scalars, we can calculate these quantities in the rest frame of the proton.

We find

$$I_1 = \frac{2\pi}{|\vec{q}|}\int_{K_1}^{K_2} d|\vec{K}||\vec{K}|\hat{P}_\mu\hat{P}_\nu\left[\left(g^{\mu\nu} - \frac{q^\mu q^\nu}{q^2}\right)(m_q A - p\cdot B) + \hat{p}^\mu\hat{B}^\nu + \hat{p}^\nu\hat{B}^\mu\right] \tag{3.23}$$

and

$$I_2 = \frac{2\pi}{|\vec{q}|}\int_{K_1}^{K_2} d|\vec{K}||\vec{K}|\left[\,3\,(\,m_qA - p\cdot B\,) + 2\hat{p}\cdot\hat{B}\,\right] . \qquad (3.24)$$

Solving Eqs. (3.20) - (3.22) for W_1 and W_2 and using Eqs. (3.23) - (3.24), we have

$$W_1(P^2, P\cdot q, q^2) = \frac{2\pi}{|\vec{q}|}\int_{K_1}^{K_2} d|\vec{K}||\vec{K}|\left[(\,p\cdot B - m_qA - \hat{p}\cdot\hat{B} + (\hat{P}\cdot\hat{p})(\hat{B}\cdot\hat{p})/(\hat{P}^2)\right] , \qquad (3.25)$$

and

$$W_2(P^2, P\cdot q, q^2) = \frac{2\pi}{|\vec{q}|}\int_{K_1}^{K_2} d|\vec{K}||\vec{K}|\left[\frac{3m^2(\hat{P}\cdot\hat{p})\,(\hat{p}\cdot\hat{B})}{\hat{P}^4} - \frac{m^2}{\hat{P}^2}(\hat{p}\cdot\hat{B})\right] . \qquad (3.26)$$

The integrals appearing in the last two equations are to be calculated in the rest frame of the proton.

We now transcribe these results to a covariant form using the substitution

$$(P^0)^2 \rightarrow P^2 , \qquad (3.27)$$

$$\nu \rightarrow (P\cdot q)/\sqrt{P^2}\ , \tag{3.28}$$

and

$$|\vec{q}| \rightarrow (P\cdot q)^2/P^2 - q^2\ . \tag{3.29}$$

3.1.2 Calculation of Structure Functions of Finite Nuclei

We can now use the resulting expressions for W_1 and W_2 to calculate the structure functions of a nucleon in a finite nucleus. Proceeding as in Eqs. (2.3) - (2.7), we write the response tensor for a target nucleus of A nucleons. (Since we want to compare the nuclear structure function per nucleon to the structure function of free nucleon, we include a factor of 1/A):

$$W^A_{\mu\nu}(P_A, q) = \frac{1}{A}\sum_{i=1}^{A}\int d^3P\,\left|\phi_i(\vec{P})\right|^2 W^N_{\mu\nu}(P, q)\ . \tag{3.30}$$

Here, $\phi_i(\vec{P})$ is the wave function of the nucleon in a single-particle orbit, labeled i, and $\left|\phi_i(\vec{P})\right|^2$ is the corresponding momentum distribution, satisfying the normalization condition:

$$\int d^3P \left|\phi_i(\vec{P})\right|^2 = 1 \ .$$

We take the target to be at rest, so that $P_A^0 = M_A$ and $\vec{P}_A = 0$. In Eq. (3.30), $W_{\mu\nu}^N(P, q)$ is the response tensor for a nucleon of four-momentum P. We write $W_{\mu\nu}^A(P_A, q)$ in terms of structure functions defined for a nucleus

$$W_{\mu\nu}^A(P_A, q) = W_1^A(P_A\cdot q, q^2)\left(-g_{\mu\nu} + \frac{q_\mu q_\nu}{q^2}\right) + W_2^A(P_A\cdot q, q^2)\,\frac{\hat{p}_\mu^A \hat{p}_\nu^A}{M_A^2} \ . \qquad (3.31)$$

Following the same procedure as that used in the case of a free nucleon, we define the invariants

$$I_1^A = W_{\mu\nu}^A \hat{P}_A^\mu \hat{P}_A^\nu \ , \qquad (3.32)$$

$$= -W_1^A \hat{P}_A^2 + W_2^A \hat{P}_A^4 / M_A^2 \ , \qquad (3.33)$$

$$I_2^A = W_\mu^{A\mu} \ , \qquad (3.34)$$

$$= -3W_1^A + W_2^A \hat{P}_A^2 / M_A^2 \quad . \tag{3.35}$$

We calculate I_1^A and I_2^A in the rest frame of the target nucleus. Using Eq. (3.30) we obtain

$$I_1^A = \frac{1}{A} \sum_{i=1}^{A} \int d^3P \left|\phi_i(\vec{P})\right|^2 \left[-\hat{P}_A^2 W_1^N + W_2^N \frac{(\hat{P}_A \cdot \hat{P})^2}{P^2} \right] , \tag{3.36}$$

$$I_2^A = \frac{1}{A} \sum_{i=1}^{A} \int d^3P \left|\phi_i(\vec{P})\right|^2 \left[-3W_1^N + W_2^N \frac{\hat{P}^2}{P^2} \right] . \tag{3.37}$$

Solving Eqs. (3.32) - (3.35) for W_1^A and W_2^A and, making use of Eqs. (3.36) and (3.37), we have,

$$W_1^A (P_A \cdot q, q^2) = \frac{1}{A} \sum_{i=1}^{A} \int d^3P \left|\phi_i(\vec{P})\right|^2 \left(W_1^N (P^2, P \cdot q, q^2) \right. \tag{3.38}$$

$$+ W_2^N (P^2, P\cdot q, q^2) |\vec{P}|^2 \frac{(1 - \cos^2\theta)}{(2P^2)}) ,$$

$$W_2^A (P_A\cdot q, q^2) = \frac{1}{A} \sum_{i=1}^{A} \int d^3P |\phi_i(\vec{P})|^2 \{ W_2^N (P^2, P\cdot q, q^2) M_A^2 \tag{3.39}$$

$$\times [3 \frac{(\hat{P}_A\cdot\hat{P})^2}{\hat{P}_A^2} - \hat{P}^2] / (2P^2\hat{P}_A^2) \} .$$

The right-hand side of the last equation is to be evaluated in the rest frame of the target nucleus, $\vec{P}_A = 0$. Note that in the scaling limit, $W_2^N/W_1^N \rightarrow 0$, so that W_1^A depends only on W_1^N in that limit. In the scaling limit, we find

$$W_1^A (x_t, Q^2) = \frac{1}{A} \sum_{i=1}^{A} \int d^3P |\phi_i(\vec{P})|^2 W_1^N(P^2, P\cdot q, q^2) , \tag{3.40}$$

$$W_2^A (x_t, Q^2) = \frac{1}{A} \sum_{i=1}^{A} \int d^3P |\phi_i(\vec{P})|^2 W_2^N(P^2, P\cdot q, q^2) \tag{3.41}$$

$$\times [P^0 - |\vec{P}| \cos\theta]^2 / P^2 ,$$

where we have introduced $x_t = Q^2/(2m\nu)$. We write

$$F_1^A(x_t) = mW_1^A(x_t, Q^2), \tag{3.42}$$

and

$$F_2^A(x_t) = \nu W_2^A(x_t, Q^2). \tag{3.43}$$

In order to obtain values for $F_1(x_t)$ and $F_2(x_t)$, we have to perform the integrals in Eqs. (3.40) and (3.41). That requires that we specify the functional relation between P^0 and $\vec{P}$. To study the effect of Fermi motion in isolation, we may put $P^0 = (\vec{P}^2 + m^2)^{1/2}$ (see Fig. 8). To study the additional effect of nuclear binding, we may use

$$P^0 = m - \varepsilon_i + \vec{P}^2/2M_{A-1} \tag{3.44}$$

where $\varepsilon_i > 0$ is the separation energy of a nucleon in orbital i.

We also require the form of the wave function, $\psi^{(s_q)}(\vec{K})$, which parameterizes the valence quark density matrix. We choose

$$\psi^{(s_q)}(\vec{K}) = \sqrt{\frac{N}{4\pi}} \begin{bmatrix} \dfrac{1}{(\vec{K}^2 + \mu^2)^2}\,\chi^{(s_q)} \\ \eta\,\dfrac{\vec{\sigma}\cdot\vec{K}}{(\vec{K}^2 + \mu^2)^2}\,\chi^{(s_q)} \end{bmatrix} \tag{3.45}$$

and take $\mu = 0.89$ GeV. (We also choose η such that the lower component accounts for 1.5 percent of the wave function normalization integral.) This choice of the quark wave function leads to a quite good fit to $F_2^p(x)_{EMC}$ for $x > 0.4$. (See Fig. 9.) (A fit for $F_2^p(x)$ for smaller values of x requires that we create a model of the quark 'sea'. We will defer a discussion of the quark sea to section 3.1.3. Here we limit ourselves to a microscopic calculation of the valence quark contribution to F_1 and F_2.) Note that our use of the words 'valence' and 'sea' is not the same as that of the parton model. For example, our 'valence' quarks are off-mass-shell, while 'valence' partons are on-mass-shell objects.

In Fig. 10 we present the results of our calculation of $F_2^p(P^2, x, Q^2)$, the proton structure function, for $Q^2 = 10\ \text{GeV}^2$. For $x < 0.7$, that value of Q^2 is sufficient to achieve scaling. That is, for $Q^2 > 10\ \text{GeV}^2$, power-law corrections to scaling behavior may be neglected in our model, if x is not too

large. (That feature is described in great detail in the sixth item listed in Ref. 38. We have not attempted to calculated perturbative QCD corrections which would lead to logarithmic corrections to scaling.) As may be seen in the figure 10, there is some reduction in $F_2(P^2, x, Q^2)$ when $P^2 < m^2$ (This feature is lost in the convolution formulas of the parton model, since in that model the structure functions depend on only two variables, x and Q^2.) The two groups of dashed curves appearing in Fig. 10 will be described in the following discussion.

To understand the role $F_2(P^2, x, Q^2)$ plays in our calculation, in Fig. 10 we have superimposed various curves which show the region sampled when performing the integral in Eq. (3.30). In general, the calculation for each shell will sample a different region. Note that x_t is fixed when performing the integral in the Eq. (3.30); the region sampled depends on the value of x_t as may be seen in Fig. 10. The set of curves on the left-hand side of the figure denote the region sampled, when $x_t = 0.22$, for each orbital of ^{40}Ca. The group of the curves on the right is obtained when $x_t = 0.70$. For a finite-nucleus wave function, $|\vec{P}|$ can be infinite; however, the figure is drawn for the case of a cut-off at $|\vec{P}|_{max} = 540$ MeV. (In the numerical calculations of the EMC effect reported here we have used $|\vec{P}|_{max} = 1$ GeV.)

We now present the results of a calculation of the EMC effect for ^{4}He, ^{12}C and ^{40}Ca using such wave functions. (See Tables 1 and 2.) In these calculations we use the approximation

$$F_2^{n,\,val}(P^2, x, Q^2) = 0.95\,(1 - 0.8x)\,F_2^{p,\,val}(P^2, x, Q^2)\ , \qquad (3.46)$$

where $F_2^{p,\,val}(P^2, x, Q^2)$ is the valence quark contribution to the off-mass-shell structure function, as calculated in our model. $F_2^{p,\,val}(P^2, x, Q^2)$ depends upon the choice of μ, in addition to the kinematic variables P^2, x and Q^2 . As discussed earlier in this work, the variables μ and b may be fixed by fitting $F_2^p(x)$ (see Fig. 9) and the electromagnetic form factor of the nucleus in question. (See Table 2.)

Results obtained for ^{4}He, ^{12}C and ^{40}Ca are shown in Figs. 11-13. Recall that the parameter μ was fixed at the value μ = 0.89 GeV and b was fixed by fitting the form factors of these nuclei. However, in the figures we do show the variation of our results due to relatively small changes in the

separation energies.

3.1.3 A Description of the Quark Sea

Thus far, we have only considered the valence quark contribution to the structure functions and have discussed the EMC effect in terms of that contribution. Since we do not have a microscopic model of the sea, we include its effects in our formalism using the following scheme.

We consider the analytic parameterizaton of the structure function $F_2^p(x, Q^2)$ given by the EMC. We write the analytic form as $F_2^p(m^2, x, Q^2)$ and define, for the purpose of this work,

$$F_2^{p,\,sea}(m^2, x, Q^2) = F_2^p(m^2, x, Q^2)_{EMC} - F_2^{p,\,val}(m^2, x, Q^2) \ . \qquad (3.47)$$

Because our calculated values of $F_2^{p,\,val}(m^2, x, Q^2)$ fit the values of $F_2^p(m^2, x, Q^2)_{EMC}$ quite well for $x > 0.4$ (see Fig 8), the function defined in Eq. (3.47) is (essentially) zero for $x > 0.4$. We now proceed to make an off-mass-shell extrapolation of the full structure function and define

$$F_2^p(P^2, x, Q^2) = F_2^{p,\,val}(P^2, x, Q^2) + F_2^{p,\,sea}(m^2, x, Q^2) . \qquad (3.48)$$

Ideally, we should perform an off-mass-shell extrapolation of the sea contribution in Eq. (3.48); however, we would require a microscopic model to perform such an extrapolation. Therefore, we will content ourselves with the use of Eq. (3.48) in our formalism.

We can perform a similar off-mass-shell extrapolation for the neutron structure function. We put

$$F_2^n(m^2, x, Q^2) = 0.95\,(1 - 0.8x)\,F_2^p(m^2, x, Q^2)_{EMC} , \qquad (3.49)$$

and recall that we had previously defined

$$F_2^{n,\,val}(P^2, x, Q^2) = 0.95\,(1 - 0.8x)\,F_2^{p,\,val}(P^2, x, Q^2) , \qquad (3.50)$$

in analogy to the definition in Eq. (3.48).

In Fig. 14 we exhibit the values of $F_2^p(x)$ used in this work. The data are taken from Ref. 40 and are averaged over Q^2. Also shown in this figure is the value we calculated for the structure function of ^{40}Ca using the model for the quark sea described in this section. (We put $F_2^{p,\,sea}(m^2, x, Q^2) = 0$ for $x \geq 0.4$ and use Eq. (3.47) for $x < 0.4$ in our

calculations.)

In Figs. 15-17, we show our results for the EMC effect in ^{4}He, ^{12}C and ^{40}Ca. The dotted curves result upon inclusion of the sea contribution, while the solid curves result from including only the valence quark contribution in our calculation. The dotted and solid curves coincide (to a good approximation) for $x_t > 0.55$. The fact that the sea contribution to the data shown in these figures is finite in the region $0.40 < x < 0.55$ is due to the effects of Fermi motion. (Recall that we had put the sea contribution equal to zero for $x \geq 0.4$ in Eq. (3.47).) We see that, particularly in the case of ^{40}Ca, we may achieve a good fit to the SLAC data.

3.1.4 Conclusions and Discussion

If one discusses the role of nuclear binding using the convolution formulas of the parton model, the results are sensitive to a single parameter, the average separation energy, $<\varepsilon>$.[11,13,21,41] Therefore, one might think that a calculation using wave functions of finite nuclei might reproduce the data

for reasonable values of $< \varepsilon >$. Here we have argued that the situation is significantly more complicated. That is, rather than using the free-space structure functions at some shifted value of x (obtained from consideration of Fermi motion) we suggest that one needs to consider a true off-mass-shell effect and to construct a model for the dependence of $W_1(P^2, x, Q^2)$ and $W_2(P^2, x, Q^2)$ on the variable P^2.

It is gratifying to note that the use of the wave functions of finite nuclei leads to a good account of the experimental data, if reasonable values are used for the oscillator parameter and for the separation energies.

One feature which emerges from this analysis appears to us to be particularly interesting. One can understand why the EMC effect appears largely as an effect involving the valence quarks of our model. The reason is that nuclear binding affects the calculation through the modification of the off-mass-shell characterization of the quarks comprising the nucleon. For the large x region, where the wave function is characterized by three valence quarks, the binding effect is relatively undiluted, being spread over three degree of freedom. In the small x region, dominated by the quark 'sea', there are many quark degrees of freedom which characterize the nucleon wave function. Therefore, the binding effect is spread over these many degrees of freedom and the (relative) modification of the off-mass-shell characterization of

a single 'sea' quark is small. These ideas can be given a more explicit formulation, if we are able to create a microscopic model of the quark sea.

3.2 The 'Swollen Nucleon' Effect

As we noted earlier, in our microscopic wave functions, there are two parameters. One of them, the mass parameter μ, which determines the form of the (valence) quark wave functions, is fixed by fitting data for $F_2^p(x)$, the structure function of the proton. We have $\mu = 0.89$ GeV. Although this choice leads to a quite good fit for $x > 0.4$, there is still a problem. In the region $0.6 \leq x \leq 0.8$, $F_2^p(x)$ in our model is about 80% of the corresponding value of the EMC data. In convolution formula, we used this $F_2^p(x)$ to calculate $F_2^A(x)$, and obtained $R_{EMC} < 1$. However, this is quite unsatisfactory, since the fact $R_{EMC} < 1$ is due to the use of this 'congenitally deficient' $F_2^p(x)$. Therefore, we use the experimental value of $F_2^p(x)$ in convolution integral. We use the analytic parameterization of the structure function $F_2^p(x, Q^2)_{EMC}$ given by the EMC. At first, we only consider

Fermi motion and binding. (Since $F_2^p(x, Q^2)_{EMC}$ is the experimental value, it is an on-shell quantity.) As expected, the EMC ratio calculated rises too early in this calculation. We again considered the off-mass shell effect. Since $F_2^p(x, Q^2)_{EMC}$ is the (on-shell) experimental value, we try to put the off-mass-shell effect in the convolution integral by multiplying $F_2^p(x, Q^2)$ a factor,

$$O = \left[\frac{W_2^p(P^2, x, Q^2)}{W_2^p(m^2, x, Q^2)} \right], \tag{3.51}$$

which will become 1 when the particle is on-shell ($P^2 = m^2$). Here, $W_2^p(P^2, x, Q^2)$ is the microscopic structure function calculated with wave functions we obtained in Section 3.1.1. But, unexpectedly, the results were even worse when the off-mass-shell effect was included.

Many people have argued,[29-31,42] that the properties of the nucleon, like its mass or size, are affected by the presence of other nucleons in a nucleus. From one point of view , nucleons swell in a nuclear environment. In our microscopic wave function, the mass parameter is closely connected to the radius R which represents the size of the nucleon,

$$\langle R^2 \rangle^{1/2} = \sqrt{3}/\mu \ . \tag{3.52}$$

That is, our wave function can be directly connected with the size of the nucleon. When $\mu = 0.89$ GeV, the calculated values of $F_2^{p,\,val}(m^2, x, Q^2)_{EMC}$ fit the values of $F_2^p(m^2, x, Q^2)_{EMC}$ quite well for $x > 0.4$. We then assume the corresponding R_0 is the radius for free nucleon. We introduce the 'swollen nucleon effect' by introducing a factor S in the convolution integral:

$$S = \left[\frac{W_2^{p,\,val}(\mu, P^2, x, Q^2)}{W_2^{p,\,val}(\mu_0, m^2, x, Q^2)} \right] , \tag{3.53}$$

This quantity is 1 when the proton is in free space. Here, $\mu < \mu_0$. We performed calculations for ^{4}He, ^{12}C and ^{40}Ca and found, if R/R_0 is about 1.05, the results are improved. The inclusion of the 'swollen nucleon effect', not only can get the required depletion at medium x region, but we also obtained an increase in the small x region for $R_{EMC}(x, Q^2)$. (See Figs. 18-20.)

As we noted earlier, in the Q^2-rescaling model, it was suggested that

$$F_2^{Fe}(x, Q^2) = F_2^D(x, \xi(Q^2)\, Q^2)_{EMC} \ .$$

It was proposed that $\xi(Q^2) = (\mu_0^2/\mu^2)^{\alpha(\mu^2)/\alpha(Q^2)}$. Using a bag model, a relation was also proposed between μ and radius R. (There are several steps in that procedure.) In the 'swollen nucleon' model, our microscopic wave function is connected directly to the size of the nucleon; therefore, the theoretical ideas have a more intuitive character and the physical significance of the model is clear.

3.3 Final State Interaction Model

In Section 3.2, when we calculated the structure function $F_2^A(x, Q^2)$ for target nuclei, we used the analytic parametrization of the structure function $F_2^p(x, Q^2)_{EMC}$ given by the EMC. We took $Q^2 = 10\,GeV^2$. Here $x = Q^2/(2P\cdot q) = x_t/y$, $y = P\cdot q/(m\nu)$. Further, $x_t = Q^2/(2m\nu)$ represents the momentum fraction carried by the quarks in the nucleon. The effects of Fermi motion are included in the factor 1/y and binding effects may also be

included by specifying the relation between P^0 and $\vec{P}$. One can assume, in addition, that the interactions between the final-state debris of the struck nucleon and the residual nucleus may be important. It is possible that the x value of the quark is degraded. If x is degraded in the final state, the structure function should be evaluated at a larger value of x. We assume that the change of x is: $x \rightarrow x' = x(1 + \delta)$. Here δ is a parameter to be determined by fitting the data for the EMC effect. After changing x to $x(1 + \delta)$ in the convolution formulas, the results are improved. Results obtained for ^{4}He, ^{12}C and ^{40}Ca are shown in Figs. 21-23. Note that this is basically a 'x-rescaling' model whose physical basis is different than that previously considered.

We found that δ has a A-dependence. For light nuclei, such as ^{4}He, δ is smaller, (about 0.02,) while for heavier nuclei, such as ^{40}Ca, a bigger δ is suitable (about 0.03 - 0.04). However, we need do more work to determine the precise relation between δ and A. An analysis of the A-dependence of δ was made by Glazek and Shakin [43] in the light-front formalism. For ^{4}He and ^{40}Ca, essentially the same values of δ were obtained in that work as

were found in our study. This provides some confidence that the extraction of δ may be independent of whether one uses the instant form of dynamics, or the light-front form. Further, we see that a study of the relation between these formalisms is needed. (The analysis of Glazek and Shakin is described in Section 3.4.)

3.4 The Light-Front Formalism

Any theory of a dynamical system has to satisfy the requirements of special relativity and exhibit Hamiltonian equations of motion. This leads to the appearance of ten fundamental quantities for each dynamical system, namely, the total energy, the total momentum and the 6-vector which has three components equal to the total angular momentum. The usual form of dynamics expresses everything in terms of dynamical variables at one instant of time, which results in especially simple expressions for six of these ten, namely the components of momentum and of angular momentum. There are other forms of relativistic dynamics in which others of the ten are especially simple, corresponding to various sub-groups of the inhomogeneous Lorentz group [44]. One form of relativistic dynamics is the so-called light front formalism.

Consider the three-dimensional surface in space-time formed by a plane wave front advancing with the velocity of light. Such a surface will be called a front for brevity. For the x-coordinate system, an example of a front is given by the equation $x_- \equiv x_0 - x_3 = 0$. We may set up a dynamical theory in which the dynamical variables refer to physical conditions on a front. This will make simple those of the fundamental quantities associated with infinitesimal

transformations of coordinates that leave the front invariant and will yield the front form of dynamics.

Light-front, or light-one (LC), coordinates are defined by the transformation

$$(x^0, x^1 , x^2 , x^3) \rightarrow (x^+, x^1 , x^2 , x^-) \tag{3.54}$$

with $x^+ = x^0 + x^3$, $x^- = x^0 - x^3$ and $\vec{x}_\perp = (x^1, x^2)$. We get a convenient notation by using the + and - suffixes as tensor indices together with 1 and 2.

The metric tensor is

$$g_{\mu\nu} = \begin{pmatrix} 0 & 0 & 0 & \frac{1}{2} \\ 0 & -1 & 0 & 0 \\ 0 & 0 & -1 & 0 \\ \frac{1}{2} & 0 & 0 & 0 \end{pmatrix} \quad ; \quad g^{\mu\nu} = \begin{pmatrix} 0 & 0 & 0 & 2 \\ 0 & -1 & 0 & 0 \\ 0 & 0 & -1 & 0 \\ 2 & 0 & 0 & 0 \end{pmatrix} . \tag{3.55}$$

where μ and ν are summed over +, 1, 2, -. Therefore the scalar product is

$$A \cdot B = \frac{1}{2}(A^+B^- + A^-B^+) - \vec{A}_\perp \cdot \vec{B}_\perp . \tag{3.56}$$

In particular, one has

$$\Box = \partial_\mu \partial^\mu = \partial^+ \partial^- - \partial^2 \ , \tag{3.57}$$

and

$$\partial^+ = \frac{\partial}{\partial x_+} = 2\,\partial_- = 2\frac{\partial}{\partial x^-} \ , \tag{3.58}$$

$$\partial^- = \frac{\partial}{\partial x_-} = 2\,\partial_+ = 2\frac{\partial}{\partial x^+} \ . \tag{3.59}$$

We use the convention that x^+ is the LC time and p^- is the LC energy.

The fundamental quantities p_1 , p_2 , p_- , M_{12}, M_{+-}, M_{1-} and M_{2-} are associated with transformations of coordinates that leave this front invariant and will be especially simple. The remaining ones p_+ , M_{1+} and M_{2+} will be complicated, in general.

Thus, the front form has the advantage that it has seven of the ten fundamental generators given by simple expressions, instead of the six of the instant form. This makes it mathematically the most interesting form. The front form has the further advantage that there is no square root in the expression for p_- , which means that one can avoid negative (LC) energies for particles by suitably choosing the value of the dynamical variables on the front. (One avoids having to make a special convention for the sign of a square root.) It may then be easier to eliminate negative energies from the quantum theory. In other words, the Einstein mass relation

$$p^2 = p_\mu p^\mu = m^2 \tag{3.60}$$

is linear in p^- and p^+, in contrast to the quadratic form in p^0 and $\vec{p}$. From the on-mass-shell relation, we get

$$p^+p^- - \vec{p}_\perp^{\,2} = m^2 \rightarrow p^- = (\vec{p}_\perp^{\,2} + m^2)/p^+ \ , \tag{3.61}$$

$$(p^0)^2 - \vec{p}^{\,2} = m^2 \rightarrow p^0 = \pm\sqrt{\vec{p}^{\,2} + m^2} \ . \tag{3.62}$$

In the above equations we should contrast not only the single solution for p^- versus the two solutions for p^0, but also the simpler, quadratic dependence of p^- on $\vec{p}_\perp$, instead of the square root dependence of p^0 on $\vec{p}^{\,2}$. Note that $p^- = (\vec{p}_\perp^{\,2} + m^2)/p^+$ is the on-shell value of the energy. Besides, in the light front approach, all particles are treated equally, since all of them are on their mass shells. The energy-momentum vector, where p^- is on shell, is written as (p^+, p_1, p_2, p^-).

In the following, we will describe final state interactions (FSI) in the light front formalism in a study of the EMC effect.

3.4.1 Final State Interaction (FSI) Model

Consider the usual convolution expression for the invariant structure function of the nucleus in the light-front formalism [45]. We have

$$F_2^A(x, Q^2) = \int_x^1 dy\, \rho_A^N(y)\, F_2^N(x/y, Q^2) , \tag{3.63}$$

where $\rho_A^N(y) = \int d^3p\, \delta(y - Ap^+/P_A^+)\, \rho_N(p)$ is the probability density that the nucleon carries longitudinal momentum fraction y of the momentum of the whole nucleus and $x = q^2/(2M\nu)$ is the Bjorken variable. Further

$$\rho_N(p) = \int d^3p < P_A | a_N^+(p)\, a_N(p) | P_A > /A \tag{3.64}$$

is the light-front momentum density of the nucleons in the target. p and P_A are respectively the four-momenta of nucleon and target. The normalization condition, $\int d^3p\, \rho_N(p) = 1$, implies

$$\int dy\, \rho_A^N(y) = 1 . \tag{3.65}$$

If nucleons are the only constituents of the nucleus, the conservation

of the light-front momentum requires $\sum_i^A p_i^+ = P_A^+$, which in turn implies

$$\int dy\, y\, \rho_A^N(y) = 1 . \tag{3.66}$$

In the presence of other hadrons, such as pions, $\sum_i^A p_i^+ < P_A^+$, which implies

$$\int dy\, y\, \rho_A^N(y) < 1 . \tag{3.67}$$

In either case, the momentum fraction p_i^+/P_A^+ is always between 0 and 1.

In the conventional picture of the nucleus, the long- and medium- range nuclear forces are dominated by one- and two-pion exchange. This picture implies the presence of constituent pions in the ground-state of the nucleus. The density describing the light-front momentum fraction of pions per nucleon

is then $\rho_A^\pi(y) = \int d^3p\, \delta(y - Ap^+/P_A^+)\, \rho_\pi(p)$, where

$$\rho_\pi(p) = \int d^3p' < p_A |\, a_\pi^+(p')\, a_\pi(p)\, | p_A > /A \quad . \tag{3.68}$$

The average number of pions per nucleon is $< n_\pi > = \int dy\, \rho_A^\pi(y)$. In the presence of pions the convolution formulae for the structure functions is

$$F_2^A(x, Q^2) = \int dy \left[F_2^N(x/y, Q^2)\, \rho_A^N(y) + F_2^\pi(x/y, Q^2)\, \rho_A^\pi(y) \right] . \tag{3.69}$$

Conservation of the light-front momentum in this case implies

$$\int dy\, y\, \rho_A^N(y) + \int dy\, y\, \rho_A^\pi(y) = 1 . \tag{3.70}$$

In order to calculate $\rho_\pi(p)$ correctly, it is necessary to know the nuclear wave function constructed on the light front. However, thus far we do not have much information about light-front nuclear wave functions. If we use the well-known instant-form nuclear wave functions, we must use equal-time quantization. Then the interpretation of the distribution functions, ρ^N and ρ^π, as

probabilities is complicated by the need to consider the dynamics of nucleons and pions explicitly. A recent analysis[46], which provides a quite good fit to the SLAC data beyond the shadowing region, requires that about three percent of the momentum in the iron nucleus be carried by mesons. However, this percentage is required to increase in heavy nuclei to explain the effect, while binding effects are expected to saturate around A = 56. There does not appear to be a natural explanation for the increasing fraction of momentum carried by mesons as one considers heavier nuclei, although we cannot exclude such growth on theoretical grounds. A satisfactory resolution of this problem again requires a systematic study of light-front nuclear dynamics which has not been performed as yet. It is therefore doubtful that pion dynamics are well treated.

At high energies, hadronization takes place at some distance from the point where the quark absorbs the energetic photon. For many of the hadrons formed, this distance is significantly larger than the radius of a large nucleus.[47] With that in mind, one may ask how the quark interacts with the medium after absorbing an energetic photon, and if this interaction may influence the structure functions of nuclei at the few percent level.

In the light of the comments, one is motivated to study the role of final-state interactions in providing a novel explanation of the EMC effect. (We remark that final state interactions, if present, are not expected to saturate at intermediate values of the mass number, as is the case of explanations based upon nuclear

binding.) For this analysis, we need only consider values of x sufficiently large so that 'shadowing' is unimportant. We also neglect any aspects of the dynamical description which would lead to corrections to the convolution formula of Eq. (3.61).

Among the various explanations of the EMC effect, as we mentioned before, none of them have addressed the role of final-state interactions. For the time being, we neglect the role of pions and consider Eq. (3.62). If we modify the above formula to include coherent final state interactions in a minimal way, so as not to invalidate the convolution formula, we have

$$F_2^A(x, Q^2) = \int_0^1 dx' \int_{x'}^1 dy\, \rho_A^N(y)\, F_2^N(x'/y, Q^2)\, P(x', x; Q^2) \quad , \tag{3.71}$$

where $P(x', x; Q^2)$ describes the relation between the x' value of the struck quark and the value of x the quark has when we consider it to be no longer interacting with the medium. We will make a simple assumption concerning the form of $P(x',x; Q^2)$ and find that the analysis of the data of Ref. 48 supports this assumption.

3.4.2 Description of Deep-Inelastic Scattering

The interpretation of structure functions in terms of the parton model relies heavily on the impulse approximation. One assumes that the quark leaves the interaction region as if it were free, having a very large energy in comparison to all spectators. The cross section may be calculated in terms of the probability to produce the quark in the final state. It is assumed that the cross section to produce the quark is equal to the cross section to produce anything; that is, hadronization takes place with unit probability at a later stage in the process and at much longer distances than that probed by the incident photon. The cross section is then expressed in terms of the probability distribution of quarks in the target, as a function of the Bjorken variable, x_{Bj}, which is identified with fraction of the target momentum carried by the struck quark. (Experimentally measured structure functions of nucleons support this idea to large extent, though recent problems in understanding polarized structure functions do not permit the conclusion that the details of proton structure are properly understood.)

If we consider a quark present in a large nucleus, we may note that after absorbing a photon, the (weakly interacting) quark may travel about several fermis through a medium of density comparable to the proton density itself before it can properly be described as a 'physical' particle for the purposes of calculating a

cross section. We suggest that the quark can interact weakly with the medium, emitting some soft radiation which can be absorbed or scattered by the particles of the medium before the quark leaves the nucleus to be counted in the final state. However, such processes can degrade the quark momentum somewhat from the value it had just after absorbing the photon. Although the quark interaction with matter is weak, it is conceivable that the quark may lose a few percent of its original momentum. This has the consequences that, when we perform calculations of the nuclear structure function, we find that we are performing an average over the Fermi motion of the target using a nucleon structure function evaluated at a slightly larger value of x than we would use otherwise. Thus the FSI model gives rise to a 'rescaling analysis' somewhat different from those considered previously. On the basis of the FSI model we expect that the shift in the value of x depends upon the quark passage through nuclear matter and we should find that the shift has a component proportional to $A^{1/3}$. That is what our data analysis suggests, providing support for the model put forth. (As noted earlier, the FSI model provides a natural explanation of why effects due to the nuclear medium do not saturate with increasing mass number.)

3.4.3 Light-Front Calculation of Deep-Inelastic Scattering

We suggest that the analysis of deep inelastic scattering is best done in the light-front formalism, although most of our understanding of nuclear dynamics has been achieved within the context of the instant form of dynamics. In spite of the lack of complete understanding of light-front nuclear dynamics, we believe the advantages of the light-front formalism for this problem make it the natural choice for this analysis.

We assume that the transverse momenta of quarks in nucleons are negligible for this discussion. We consider the projection, k^+, of the quark momentum defined with respect to the direction specified by the photon momentum and the target momenta [49]. The ratio of k^+ to the projection of the nucleon momentum, p^+, in the same direction, is called x, the longitudinal fraction of the nucleon momentum carried by the quark. In the Bjorken limit, x coincides with x_{Bj}, as in the parton model. The nucleon structure function is equal to

$$F_2^N(x_{Bj}) = \int_0^1 dx\, f(x)\, 2m\nu\, \delta(2m\nu - Q^2/x) \tag{3.72}$$

$$= \sum_i e_i^2 x_{Bj} f(x_{Bj}) \quad , \tag{3.73}$$

where f(x) is the probability of finding a quark with momentum fraction x. (Note that an integration has been performed over momentum components transverse to the direction used in defining x. For simplicity, we do not distinguish between the various valence distributions and 'sea' quark distributions.) The nuclear structure function is then equal to

$$F_2^A(x_{Bj}) = A\int_x^1 dy\, \rho_A^N(y) \int_0^y \frac{dx}{y}\, f(x/y)\, 2m\nu\, \delta(2m\nu - Q^2/(x - \Delta x)), \tag{3.74}$$

$$= A\int_{x_{Bj}(1+\Delta)}^1 dy\, \rho_A^N(y)\, F_2^N\left(\frac{x_{Bj}}{y}(1+\Delta)\right) , \tag{3.75}$$

if we make the assumption that the quark loses a fraction Δ of its light-front momentum, characterized by the value of x. Here $\rho_A^N(y)$ represents the probability to find a nucleon carrying fraction y of the momentum of nucleus.

In general, the shift Δ may be a function of x, Q^2, or even ν; however, we will assume that $\Delta = \Delta(A, Q^2)$. The simplest assumption is that the change

in x depends upon the magnitude of x. That is, we assume that the quark loses a fraction Δ of its x value.

We note that the authors of Ref. 48 state that their data is largely Q^2 independent and they present data averaged over several values of Q^2. We, therefore, also assume that the data we are studying are independent of Q^2; however, we find that our parameterization of the final-state interaction effect, via the parameter $\Delta(x, Q^2)$, is Q^2 dependent. This unusual feature has its origin in the fact that the nucleon structure functions used are themselves Q^2 dependent. Thus, there is a complex interplay between our parameterization via $\Delta(x, Q^2)$ and the scaling violations exhibited by the nucleon and deuteron structure functions themselves.

We have taken the nucleon structure function to be the structure function for a nucleon in vacuum. That is, we neglect off-mass-shell corrections. In the past, off-mass-shell effects have been considered within the context of the instant form of dynamics. There is a good deal of arbitrariness in the use of the instant form and the techniques applied in that formalism have been subject to some criticism [50]. (Usually, some confusion is created when features of instant dynamics and light-front dynamics appear in the same calculation.) While neither formalism is free of ambiguities, we will here limit ourselves to the light-front

analysis. Ultimately, we would hope that both formalisms are well enough understood that the same result could be obtained on the basis of the same physical assumptions. In part, some of our difficulties lie in our lack of understanding in how to use Feynman diagrams in nuclear physics in an optimum manner, such as to obtain a level of accuracy necessary for calculation of the EMC effect. (Some discussion of off-mass-shell effects in a specific, simple model, as they appear in the light-front formalism, may be found in Ref. 49.)

Finally, we need to specify the nuclear momentum distribution, $\rho_A^N(y)$. Again we face the problem that this function is not measured directly . That function is properly defined in terms of the modulae squared of light-front wave functions, summed over light-front (effective) Fock-space sectors in the nucleus, and integrated over all degrees of freedom except y. We believe that it is quite reasonable to assume that $\rho_A^N(y)$ has its support well located around $y = 1/A$ and its width given, approximately, by the known Fermi momentum of nucleons in a nucleus. Moreover, $\rho_A^N(y)$ is normalized to 1, since it represents a single nucleon distribution. We also require that the first moment of y, $\langle y \rangle_\rho = 1/A$. This is consistent with our assumption that binding fields carry little of the total momentum. In this assumption, the FSI model differs in spirit

from the models of Refs. 46 and 51 . Nevertheless, the FSI model is similar to various 'rescaling' models. We note that, in general, some type of rescaling model may be used to fit the data. The important issue is, of course, the dynamics underlying a rescaling analysis.

Since the model used is quite simple, we have also chosen a simple form for $\rho_A^N(y)$. We put

$$\rho_A^N(y) = \frac{6\,(y_2 - y)\,(y - y_1)}{(y_2 - y_1)^3} \quad , \tag{3.76}$$

where

$$y_1 = (1 - k_F/m)/A \quad , \tag{3.77}$$

$$y_2 = (1 + k_F/m)/A \quad . \tag{3.78}$$

We infer values of k_F using the compilation of nuclear radii given in Ref. 52. (A similar shape for $\rho_A^N(y)$ was used in Ref. 53.)

The distribution chosen for $\rho_A^N(y)$ has the property that

$$m^2 < (Ay - 1)^2 > \; = \; m^2 \int_0^1 (Ay \; - \; 1)^2 \, \rho_A^N(y) \, dy \, , \tag{3.79}$$

$$= \; k_z^2 \quad , \tag{3.80}$$

$$= \; \vec{k}^2/3 \quad , \tag{3.81}$$

$$= \; k_F^2/5 \quad , \tag{3.82}$$

as expected in a nonrelativistic system.

3.4.4 Determination of $\Delta(A, Q2)$ from Deep-Inelastic Scattering

Data for $A \geq 4$

We make use of the data of Ref. 48 , since that work presents results for several nuclei. The SLAC data tables [48] present ratios of cross sections, σ_A/σ_D, as functions of x. We identify these ratios with F_2^A/F_2^D, also making use of the assumption that the quantity R has no significant dependence on A. (If these assumptions are incorrect, our analysis would have been reconsidered.)

In order to calculate F_2^A, we need to know both the proton and neutron structure functions. There are different ways of extracting the neutron structure function from the deuteron and proton data to be found in the literature and these procedures do not give identical results. (Some discussion of this matter and references to earlier literature may be found in Ref. 49.) We note that nucleon structure functions described in Refs. 54 and 55 differ by more than 10 percent for $x > 0.3$. This feature requires that we adopt a meaningful calculational strategy, since the EMC effect is of the order of ten percent. A consistent procedure appears to require that we use only a single set of data and, therefore, we only make use of the SLAC data of Refs. 48 and 54. The situation is still not entirely satisfactory, since in the SLAC analysis an adjustment was made for the neutron excess, using the relation $\sigma_n = (1 - 0.8x)\,\sigma_p$. If this approximation is used for the structure functions, it leads to a result for the neutron structure function that is as much as 5 percent larger than the neutron structure function extracted originally, the deviation varying with the value of x. Further, we note that the work of Ref. 54 leads to a neutron structure function which is larger by 3 percent at $x = 0$ and smaller by 1.5 percent at $x = 0.15$ from the results obtained using the simplified smearing formula described in Section 3.4.2. For x larger than 0.3, if we use, for example, $k_F = 70$ MeV and $\Delta = 0.0065$, we are able to reproduce the

relations between F_2^D, F_2^p, and F_2^n given in Ref. 54 with an accuracy better than 0.5 percent. Therefore, we conclude that there is about a 1 percent uncertainty in the theoretical results that we are not able to improve upon.

With these considerations in mind, we use the data of Ref. 54 and put

$$F_2^N(x, Q^2) = \frac{F_2^p(x, Q^2) + F_2^n(x, Q^2)}{2} . \tag{3.83}$$

There is some dependence on Q^2, with expansions of the form

$$F_2(x, Q^2) = x\,\omega \sum_{i=3}^{7} C_i (1 - \frac{1}{\omega})^i , \tag{3.84}$$

given in Ref. 54 for F_2^D, F_2^p, and F_2^n. (Values for the C_i and ω may be found in Ref. 54.)

We form the ratios

$$r(x) = \frac{\frac{1}{A} F_2^A(x/A)}{\frac{1}{2} F_2^D(x/2)} , \tag{3.85}$$

where $F_2(x)$ was given in Section 3.4.2. We then vary $\Delta(A, Q^2)$ to obtain a best fit to the data of Ref. 48 by minimizing the χ^2 value. Results obtained in this manner are given in Figs. 24 and 25. In Fig. 24, we present values of $\Delta(A, Q^2)$ for $Q^2 = 5, 10$ and 15 $(GeV)^2$. It is clear from Fig.24 that $\Delta(A, Q^2)$, determined as described above, grows with A and decreases with Q^2. The fact that Δ is proportional to $A^{1/3}$, to a good approximation, tends to confirm our original suggestion that the fraction of longitudinal momentum lost has a component proportional to the distance traveled by the quark in the medium. The fact that $\Delta(A, Q^2)$ decreases with Q^2 is interesting and may have something to do with asymptotic freedom; however, we can not be precise upon that point. The fact that $\Delta(A, Q^2)$ decreases with Q^2 in our analysis has its basis in the fact that we treat the data describing the EMC effect as being independent of Q^2. Since the nucleon structure function changes more rapidly with x for the larger values of Q^2, smaller shifts are required to fit the data at the larger values of Q^2. It is of interest to obtain greater understanding of the dependence of Δ upon Q^2. (That would require data at higher values of Q^2.)

In Fig. 25 we see the quality of the fits obtained in this model. The

analysis leads to the curves in Fig. 24, which can be fit with the form

$$\Delta(A,Q^2) = a(Q^2) + b A^{1/3} , \qquad (3.86)$$

where $a(Q^2)$ is a decreasing function of Q^2. (For example $a = 0.023$, $a = 0.015$, and $a = 0.013$ for $Q^2 = 5$, 10 and 15 $(GeV)^2$, respectively.) The quantity b is less Q^2-dependent and can be said to take on values between $b = 0.07$ (at $Q^2 = 15$ GeV ^{2}) and $b = 0.08$ (at $Q^2 = 5$ GeV ^{2}), with about a 20 percent uncertainty. With the use of a simple formula for the nuclear radius, $R(A) = r_0 A^{1/3}$, one could conclude, on the basis of the analysis presented here, that an energetic quark moving in nuclear matter loses about 1 percent of longitudinal momentum when traversing a distance of about 1 fermi.

As may be seen from Fig. 25, the fits to the data are not excellent. The value of χ^2 ranges from about 1 in ^{4}He to almost 3 for ^{56}Fe, which is the worst case. It is not possible for us to achieve a better fit for $x < 0.3$ using the nucleon and deuteron structure functions of Ref. 54. (In Ref. 49, the mesonic contribution served to increase the calculated ratio in the region $x \leq 0.4$ and, therefore, the χ^2 obtained was superior to that found here.) Surprisingly, the results for $\Delta(A, Q^2)$ are rather independent of the data

in the region $x \leq 0.4$. For example, if we either minimize the χ^2 value for all data points, or only for the data in the region $0.38 < x < 0.78$, we obtain values for Δ which differ only by a few percent. On the other hand, excluding the low x region improves the value of χ^2 by 30-50 percent. We note that the dependence on A obtained for Δ in this work matches to a large degree the A dependence of the quantity

$$< y >_\pi \; = \; \int_0^1 dy \; y \; \rho_A^\pi(y) \tag{3.87}$$

introduced in Ref. 46. ($\rho_A^\pi(y)$ is the distribution of the momentum of the pions in the nucleus that was used in Ref. 46.) This is not unexpected, since the FSI model and the model of Ref. 46 are both rescaling models, which differ mainly in their interpretation. These models may be distinguished, however, in their implications for momentum sum rules.

Another feature of our analysis is the possible dependence of the fitted values of Δ upon the choice of the nucleon distribution, $\rho_A^N(y)$, and, in

particular, upon the choice of k_F^A. However, as already noted in Ref. 49, if $\rho_A^N(y)$ is concentrated around $y = 1/A$, the results of this calculations are only sensitive to the first two moments $<(Ay-1)>$ and $<(Ay-1)^2>$. We find that, if we vary k_F^A by 5 percent, the value of Δ changes by less than 5 percent. We are encouraged by the fact that the best values for χ^2 are obtained, if we use the values of k_F^A in the range inferred from our knowledge of nuclear sizes [52].

In Ref. 46, a model with explicit mesonic degrees of freedom was considered. In that model, the presence of 'excess mesons' leads to a shift in the distribution of nucleons, $\rho_A^N(y)$. Note that $\rho_A^N(y)$ is a sharply peaked function and shifting it toward smaller values of y leads to a reduction of $<y>_\rho$ from its 'unshifted' value, 1/A. In general, such 'shifts' are not equivalent in their action to the final-state interaction discussed here. However, because of the forms of $\rho_A^N(y)$ and $F_2^N(x)$, and the fact that $F_2^N(x/y)$ appears in the convolution formula, we can see that shifting y to smaller values is equivalent to shifting x to larger values. Therefore, it can be seen that the model of Ref. 46 and the model considered here may both be characterized as 'rescaling' models. Of

course, the physical interpretation is different in both cases.

In present analysis, the observation that Δ grows as $A^{1/3}$ is found to be stable against various modifications of the theoretical formula for the ratio of the structure functions, although the use of various procedures can change the value of the parameters a and b by somewhat less than 30 percent. To reach this conclusion, we investigated various fits to the nucleon structure functions and also calculated 'Fermi smearing' in the deuteron using the above formalism. We also considered non-zero values of Δ in the case of the deuteron. If we put $\Delta_D = 0.005$, we found about a 20 percent reduction in the value of $\Delta(A, Q^2)$ for other nuclei.

Finally, one may note from inspection of the figures, that there is some tendency of the values of Δ to grow with A less rapidly for $A > 40$. Therefore, it is important for the analysis that the value of the EMC effect in Au is as large as it is. It appears that the results could be put on a firmer foundation if more accurate data were available for heavier nuclei. We would also hope to make a more refined calculation of the correction due to the neutron excess in heavier nuclei, since the correction as presently made is somewhat imprecise.

One prediction of the FSI model is that the EMC effect would be enhanced as we investigate nuclei still heavier than gold. On the other hand, because we are considering effects at the level of several percent, it will be difficult to verify our ideas by studying momentum distributions of final-state hadrons.

Another prediction of the FSI model is that final state interactions lead to an apparent violation of quark-parton momentum sum rules, while preserving other sum rules based upon probability conservation. Consider the expression for the nuclear structure function and note that $F_2^A(x)$ is negligible for $x > (2/A)$. Then we have

$$\int_0^1 dx\, F_2^A(x, Q^2) = \int_0^{1-\Delta} dx\, F_2^A(x, Q^2) \tag{3.88}$$

$$= (1 - \Delta) \langle A_y \rangle_p \int_0^1 dx\, F_2^A(x, Q^2) \tag{3.89}$$

$$= (1 - \Delta)\, P_q(Q^2)\,, \tag{3.90}$$

where we have taken, in correspondence with our previous assumptions,

$$\langle A_y \rangle = A \int_0^1 dy\, y\, \rho_A(y)\,, \tag{3.91}$$

$$= 1, \tag{3.92}$$

and used $P_q(Q^2)$ to denote the charge-weighted momentum carried by quarks in a nucleon. From Eq. (3.8) we see that final-state interactions lead to an apparent violation of the momentum sum rule obtained from the parton model. On the other hand, we have the probability relation

$$\int_0^1 \frac{dx}{x} F_2^A(x) = A \langle 1 \rangle_p \int_0^1 \frac{dx}{x} F_2^N(x)\,, \tag{3.93}$$

which properly relates the number of quarks in nucleons and in nuclei under the assumption that nuclei are composed of nucleons. We see therefore, that the FSI model predicts that the momentum sum rules are not saturated by nuclear structure functions, although probability relations are preserved. This feature has its origin in the fact that the experiment does not measure the "true" momentum distribution of quarks, but rather a degraded distribution. On the other hand, quarks are not absorbed in this model and therefore probability is conserved. (These comments presuppose that the fraction of momentum carried by gluons is unchanged in the nuclear environment. If that fraction were to change in an

unknown manner, we could not introduce a momentum sum rule for quarks alone. Further, any attempt to check momentum sum rule for quarks requires that we have a good understanding of "shadowing".) The recent experimental data of CERN [56] shows that the momentum sum rule for quarks exhibits an apparent violation in nuclei. For example, for structure functions measured per nucleon,

$$\frac{\int_0^1 F_2^A(x)\,dx - \int_0^1 F_2^D(x)\,dx}{\int_0^1 F_2^D(x)\,dx} \approx -0.023 \tag{3.94}$$

in the case of ^{40}Ca. This was already predicted in the FSI model.

One difficulty in this interpretation is that the SLAC experiment [47] was carried out at relatively low values of Q^2. Under these circumstances it is believed that some of the final hadrons are produced inside the target nucleus.

Although there are difficulties, we should note the possibility that the explanation of the EMC effect described here could be relevant to understanding the effect.

Chapter 4

Perspectives

The existing experimental information is still too scarce and uncertain to enable us to decide which of the many models, proposed to explain the EMC effect, is correct. The decrease of the nuclear structure function at medium x can qualitatively be described by nearly any class of models such as those based upon the convolution formula with contributions of 'swollen' nucleons, pion-exchange, multi-quark clusters, quark exchange. Also there exist a number of x-rescaling and Q^2-rescaling models. This just tells us that inclusive data from this x region alone is insufficient to discriminate between different explanations. Unfortunately, there is no single 'key' measurement which would allow us to clarify the situation. Therefore, we have to study many different aspects of nuclear effects in deep inelastic scattering, such as:

1) the behavior of the nuclear structure function at small x
   ($0.001 < x < 0.2$) compared to that of a 'free' nucleon:
   a) the x dependence,
   b) the A dependence and
   c) the Q^2 dependence.
2) the A dependence of

a) the sea quark distribution,

b) the gluon distribution.

3) nuclear effects in $R = \sigma_L/\sigma_T$,

4) the Q^2 dependence of F_2^A/F_2^D for $x > 0.3$,

5) the behavior of $F_2^{A_1}/F_2^{A_2}$ for $x > 1$. (This region is thought to be best suited for studying effects of nucleon-nucleon correlations or multi-quark clusters.)

6) F_2^n/F_2^p for nuclei. Such a measurement will show whether nuclear effects are the same for the neutron and the proton.

7) the influence of the nuclear medium on hadron distributions in the final state.

The information from these experiments might be sufficient to lead to a better understanding of how the nuclear environment influences the quark and gluon distributions in nuclei and would help to develop a fundamental understanding of nuclear forces in terms of quarks and gluons and their interactions.

However, all our discussion so far has dealt with spin averaged scattering. Thus $W_{\mu\nu}$ in Eq. (2.2) is symmetric and is defined with an average over the

spin of the nucleon |N> (or nucleus |A>). Experiments using polarized targets should provide very interesting information about the structure of the nucleon in terms of its constituent partons and concerning the spin structure of QCD which, modifies the parton model results. For the collision of polarized leptons with a polarized nucleon described by a covariant spin vector S_μ, the anti-symmetric part of $W_{\mu\nu}$ plays a role. We have

$$W^{em}_{\mu\nu}(S) = W^{(S)}_{\mu\nu}(S) + W^{(A)}_{\mu\nu}(S) ,$$

where $W^{(S)}_{\mu\nu}(S)$ is a symmetric second-rank tensor as given by Eq. (2.2) and anti-symmetric term is

$$W^{(A)}_{\mu\nu}(S) = \varepsilon_{\mu\nu\gamma\delta}\, q^\gamma \Big(S^\delta \Big[mG_1(\nu,q^2) + \frac{P\cdot q}{m} G_2(\nu,q^2) \Big] - P^\delta \frac{S\cdot q}{m} G_2(\nu,q^2) \Big).$$

The new structure functions, G_1 and G_2, simplify in Bjorken limit,

$$\lim m^2\nu G_1(\nu, Q^2) \Rightarrow g_1(x) ,$$

$$\lim m\nu^2 G_2(\nu, Q^2) \Rightarrow g_2(x) .$$

These structure functions depend on the spin wave function of the constituents of the hadron. If we extend the models which explain the original EMC effect to describe spin dependent quantities, for example, g_1 and g_2, it is possible that we can develop an argument, that can help to test some of models. g_1 for proton is already measured, and g_2 for the nucleon is calculable. Using the operator product-expansion and convolution formulae, g_1 and g_2 for a

nucleus are also calculable. If we calculate them for a nucleus with the same methods as those being used in explain the original EMC effect, then the various hypotheses can be differentiated by the new results and be checked by the future observation. If the results of the calculation for spin dependent structure functions are compatible with the hypothesis used in explaining the original EMC effect, then the original hypothesis would get new support.. On the other hand, if some of the original ideas are refuted by new results, we can reduce the possible candidates for explaining EMC effect.

Table 1

Momentum-Space Oscillator Wave Function

$$R_{1s}(p) = \frac{b^{3/2}}{\pi^{1/4}} 2 \exp\left[-\frac{1}{2} (bp)^2 \right] ,$$

$$R_{1p}(p) = \frac{b^{3/2}}{\pi^{1/4}} 2\sqrt{\frac{2}{3}} (bp) \exp\left[-\frac{1}{2} (bp)^2 \right] ,$$

$$R_{1d}(p) = \frac{b^{3/2}}{\pi^{1/4}} \frac{4}{\sqrt{15}} (bp)^2 \exp\left[-\frac{1}{2} (bp)^2 \right] ,$$

$$R_{1d}(p) = \frac{b^{3/2}}{\pi^{1/4}} \sqrt{\frac{8}{3}} \left[\frac{3}{2} - (bp)^2 \right] \exp\left[-\frac{1}{2} (bp)^2 \right] .$$

Table 2

Oscillator Parameters

	b (GeV^{-1})
^{4}He	6.35
^{12}C	7.6
^{40}Ca	8.5

Figure 7. Deep-inelastic scattering in the one-photon-exchange approximation. The four momentum of the photon is $q = (\nu, \vec{q})$. The nucleon four momentum is P and the nucleon spin and isospin projections are s and t. The residual system (a 'diquark') has four momentum $K = (E_d(\vec{K}), -\vec{K})$, where $E_d(\vec{K}) = (\vec{K}^2 + m_d^2)^{1/2}$, and spin angular momentum S, with projection M_S, etc. The struck quark has momentum $P - K$ before and $p = P - k + q$ after absorption of the photon. The spin and isospin projections of the quark in the final state are s_q and t_q, respectively. Here a and a denote color indices of the residual system and the struck quark.

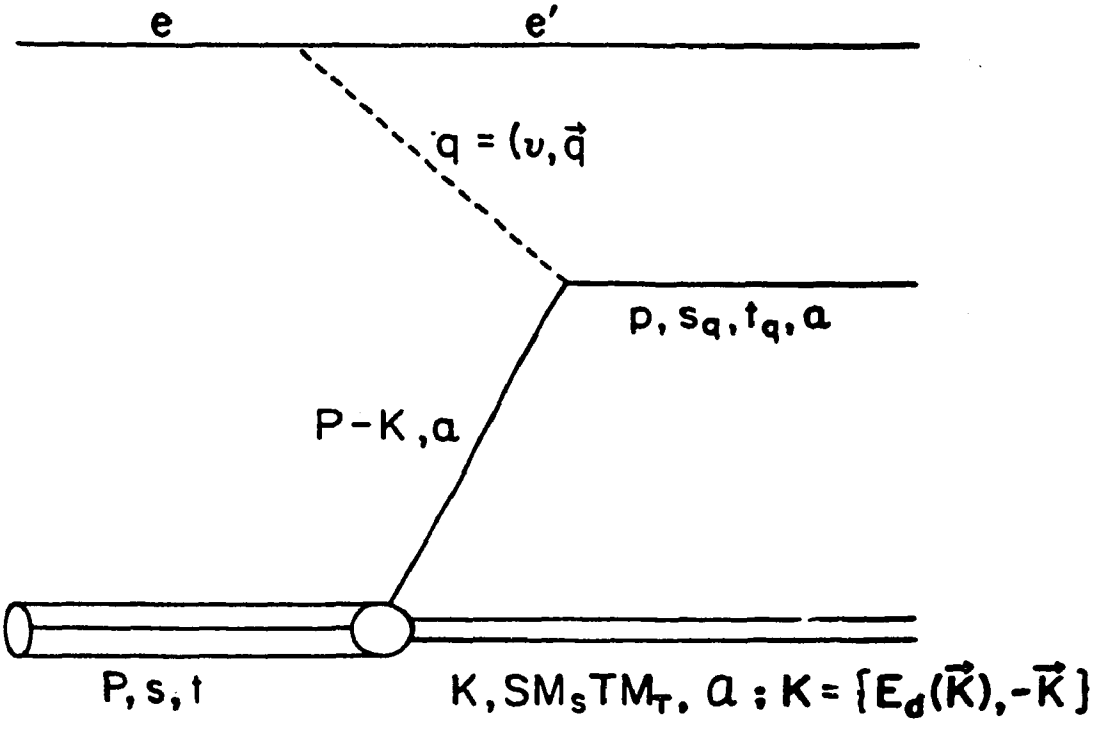

Figure 7

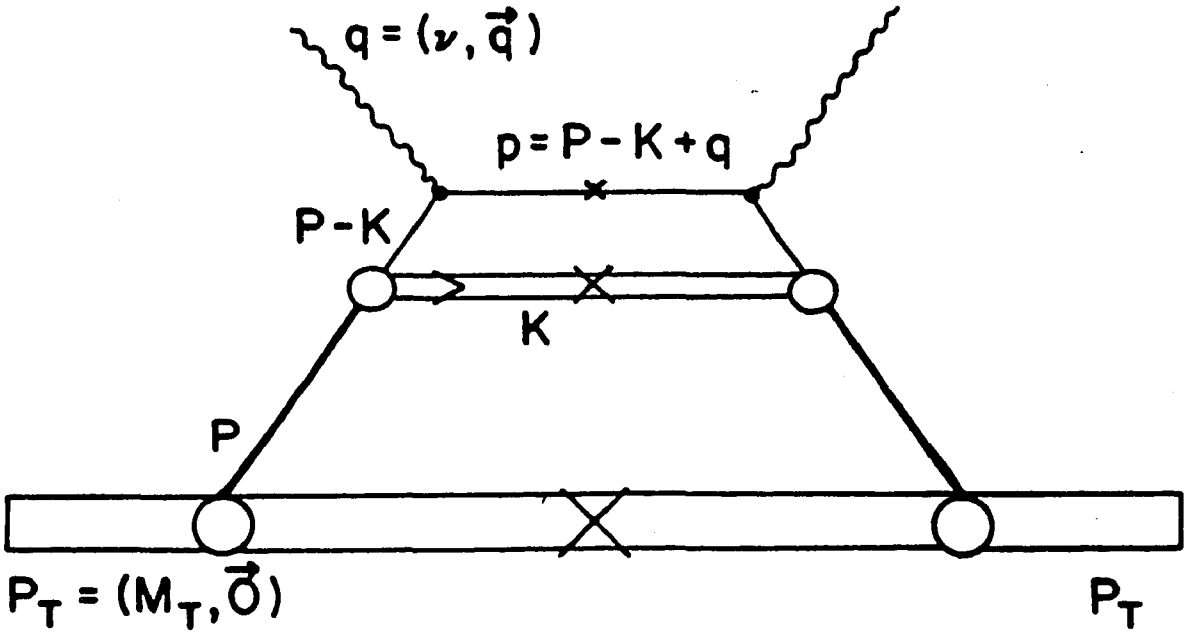

Representation of the calculation of the structure function of a large nuclear target in the target rest frame. The figure represents the imaginary part of the (virtual) forward Compton amplitude. Here, the solid line denotes an off-mass-shell nucleon of momentum $P = (P^0, \vec{P})$. In the case of nuclear matter $|\vec{P}| \leq k_F$ and $P^0 = B + \left[\vec{P}^2 + (m + A)^2\right]^{1/2}$. The upper part of the figure is parameterized as in Fig. 7, with $K = (E_d(\vec{K}), -\vec{K})$ again denoting the four-momentum of the residual system, while $p = P - K + q$ is the four- momentum of on-mass-shell quark.

Figure 8

Figure 9. 1) The solid curve denotes the analytic fit to $F_2^p(x, Q^2)$ given by the EMC [37] and evaluated at $Q^2 = 10\,(\mathrm{GeV})^2$. That form is

$$F_2^p(x, Q^2) = \left[C_1 x^{C_2}(1-x)^{C_3} + C_4(1-x)^{C_5} \right]\left(1 + \left[C_6(1-x)^{C_7} + C_8\right]\ln(Q^2/3) \right),$$

with $C_1 = 3.373$, $C_2 = 0.985$, $C_3 = 3.688$, $C_4 = 0.276$, $C_5 = 10.629$, $C_6 = 0.282$, $C_7 = 8.995$, and $C_8 = -0.078$.

2) The result of our calculation of the valence contribution to the proton structure function for $\mu = 0.89$ GeV and $m_d = m$. (See Eq. (3.45).) The parameter η is such that the lower component accounts for 1.5 percent of the normalization integral. (The fit shown was obtained upon variation of the value of μ.)

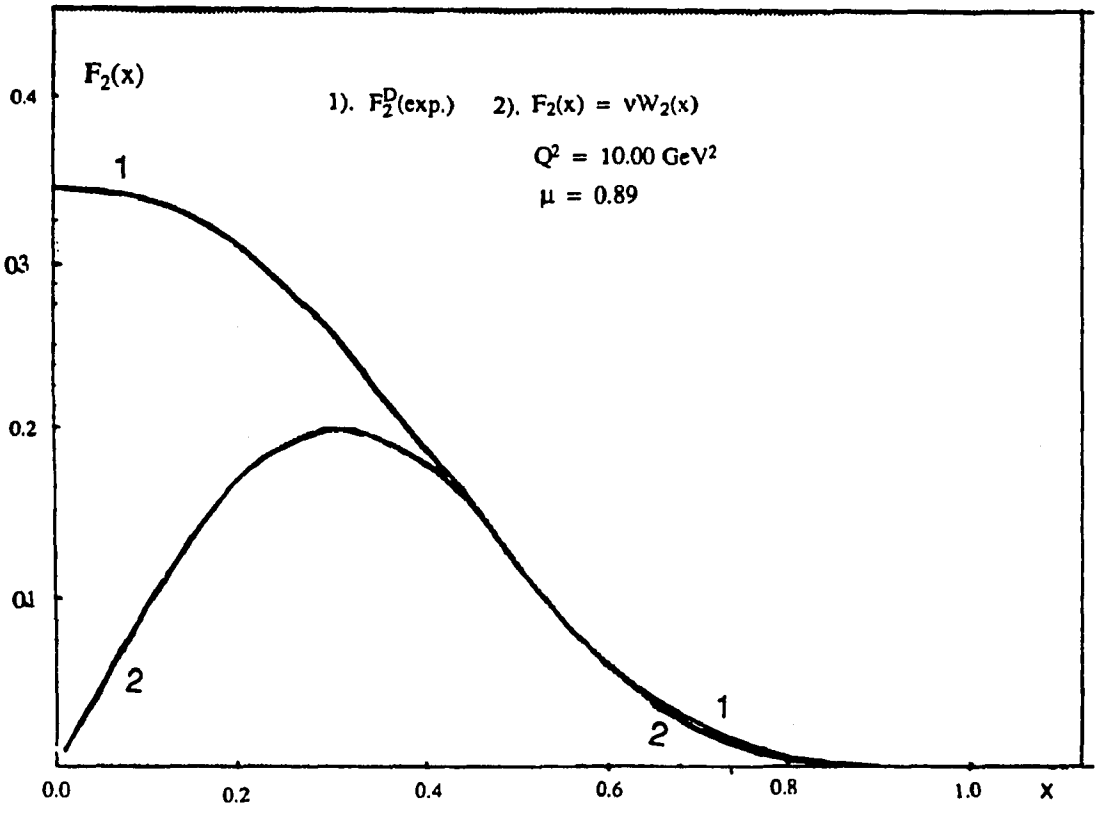
$F_2(x)$
1). F_2^D(exp.)
2). $F_2(x) = \nu W_2(x)$
Q^2 = 10.00 GeV^2
μ = 0.89
0.4
03
0.2
01
1
2
1
2
0.0
0.2
0.4
0.6
0.8
1.0
X

Figure 9

Figure 10. Off-mass-shell dependence of the valence quark contribution to the proton structure function $F_2(P^2, x, Q^2)$ calculated using the formalism of Ref. 38. (The calculation is made for $m_d = \sqrt{P^2}$ and $\mu = 0.89$ GeV.) The dotted line represents the domain of the valence quark contribution to the free-space structure function: $F_2^p(x, Q^2) = F_2^p(m^2, x, Q^2)$. The thin curves encompass the regions sampled for each orbital in our calculation of $F_1(x_i, Q^2)$ and $F_2(x_i, Q^2)$ for ^{40}Ca. The group of thin curves on the left corresponds to $x_i = 0.22$, while the group on the right-hand side is obtained for $x_i = 0.70$. Note that when $x_i = 0.70$ the kinematic domain sampled includes values of $x > 1$, where $F_2(P^2, x, Q^2) = 0$. (For the purposes of constructing this figure we have taken the maximum of $|\vec{P}| = 540$ MeV; however, in our calculations of the EMC effect in finite nuclei we have chosen the upper limit of our integrals over $|\vec{P}|$ to be 1 GeV.)

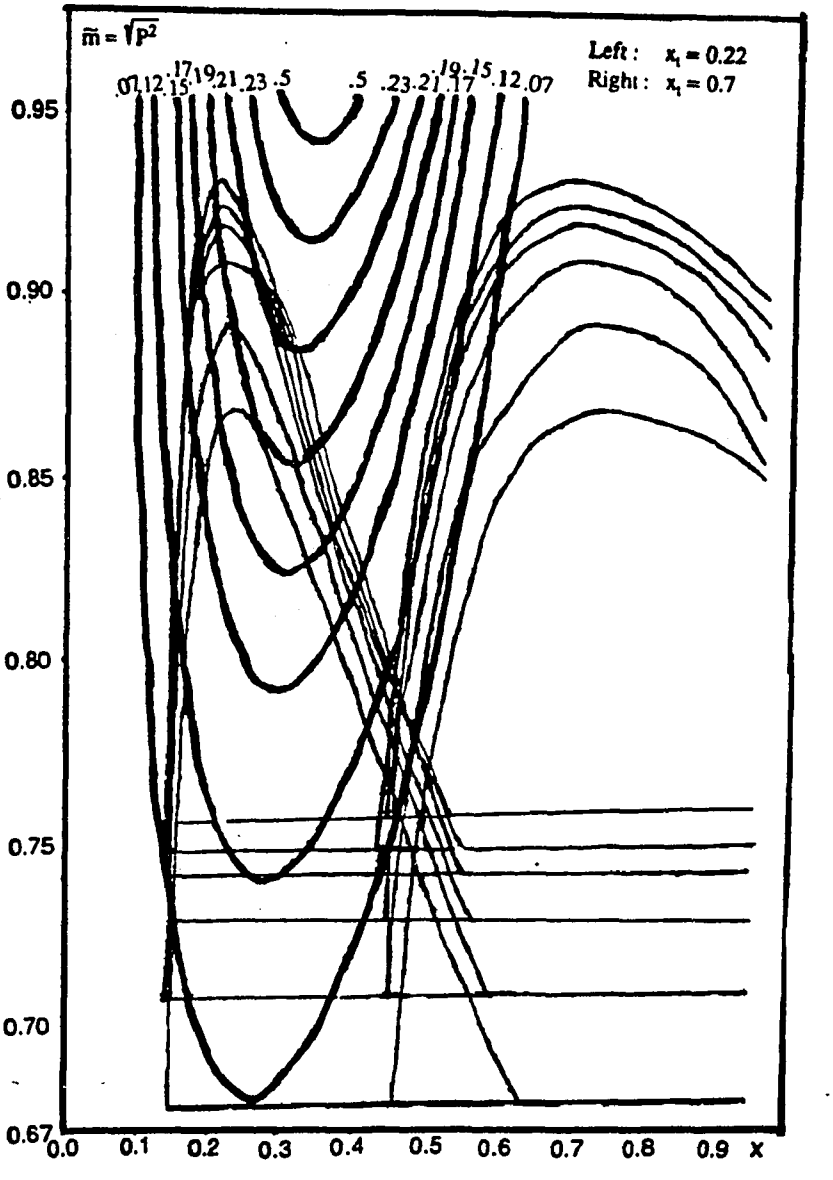
$\tilde{m} = \sqrt{P^2}$
Left: $x_1 = 0.22$
Right: $x_1 = 0.7$
.07 .12 .15 .17 .19 .21 .23 .5 .5 .23 .21 .19 .17 .15 .12 .07
0.95
0.90
0.85
0.80
0.75
0.70
0.67
0.0 0.1 0.2 0.3 0.4 0.5 0.6 0.7 0.8 0.9 x

Figure 10

Figure 11. The solid line shows the ratio of the (averaged) structure function, calculated for ^{4}He, to the experimental data[40] for the structure function of the deuteron. The deuteron data is averaged over several values of Q^2, as in Ref. 55. The calculation is made for $b = 6.35\ \mathrm{GeV}^{-1}$ and $\mu = 0.89\mathrm{GeV}$. Note that the oscillator parameter, b, refers to a wave function of relative motion, so that our value of b is equal to A/(A - 1) times the value b would have in the standard oscillator shell model. The result is shown for two values of the separation energy:

1) $\varepsilon(1s_{1/2}) = 10\ \mathrm{MeV}$,

2) $\varepsilon(1p_{1/2}) = 15\ \mathrm{MeV}$.

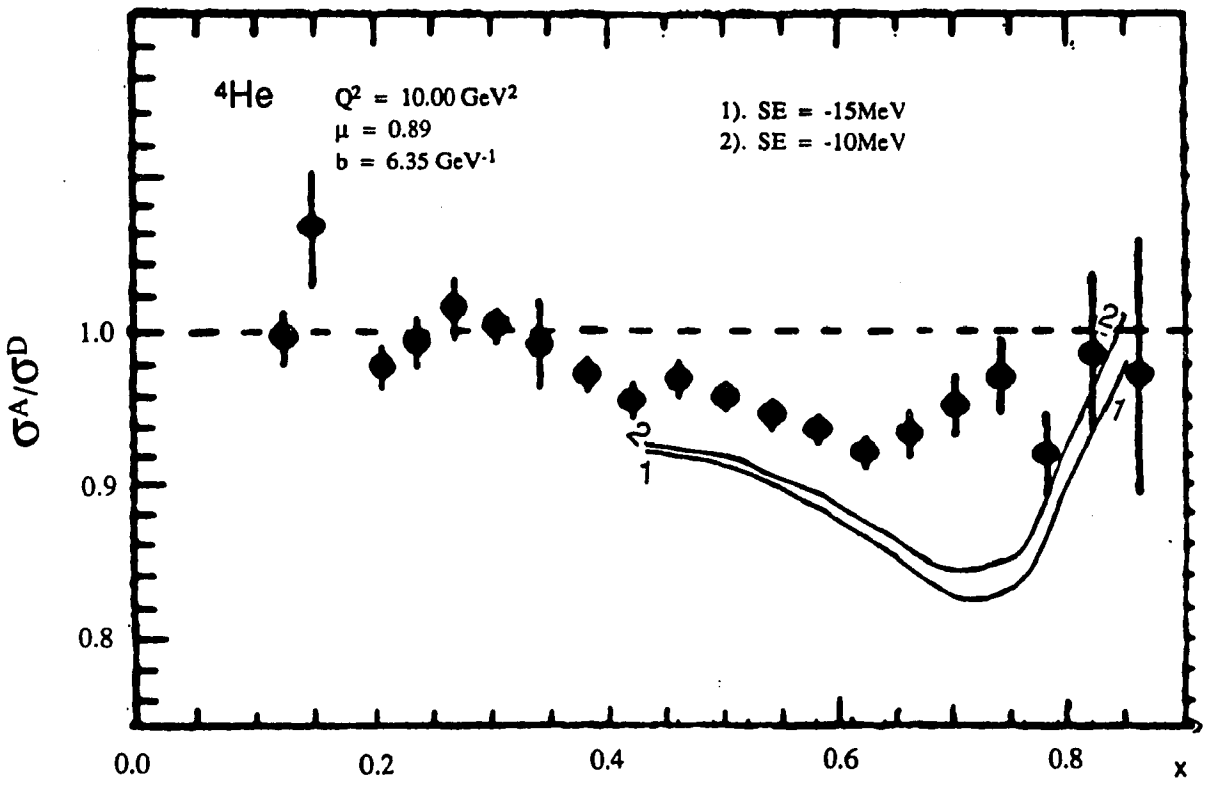
^{4}He
Q^2 = 10.00 GeV^2
μ = 0.89
b = 6.35 GeV^{-1}
1). SE = -15MeV
2). SE = -10MeV
σ^A/σ^D
1.0
0.9
0.8
0.0
0.2
0.4
0.6
0.8
x
1
2
1
2

Figure 11

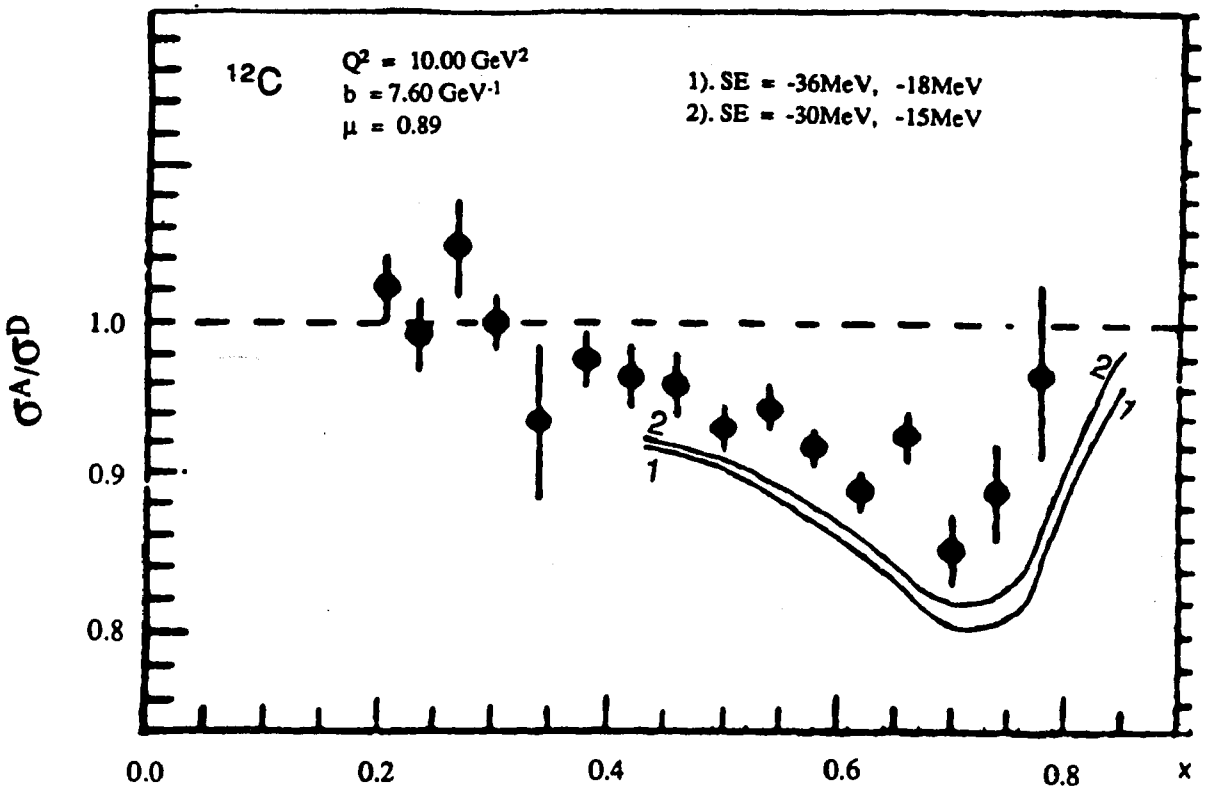

Same caption as Fig. 11, except that the target is ^{12}C. Here b = 7.6 GeV^{-1}, μ = 0.89 GeV. Results are given for two choices of the separation energies:

1) $\varepsilon(1s_{1/2}) = 36$ MeV, $\varepsilon(1p_{1/2}) = 18$ MeV,

2) $\varepsilon(1s_{1/2}) = 30$ MeV, $\varepsilon(1p_{1/2}) = 15$ MeV.

Figure 12

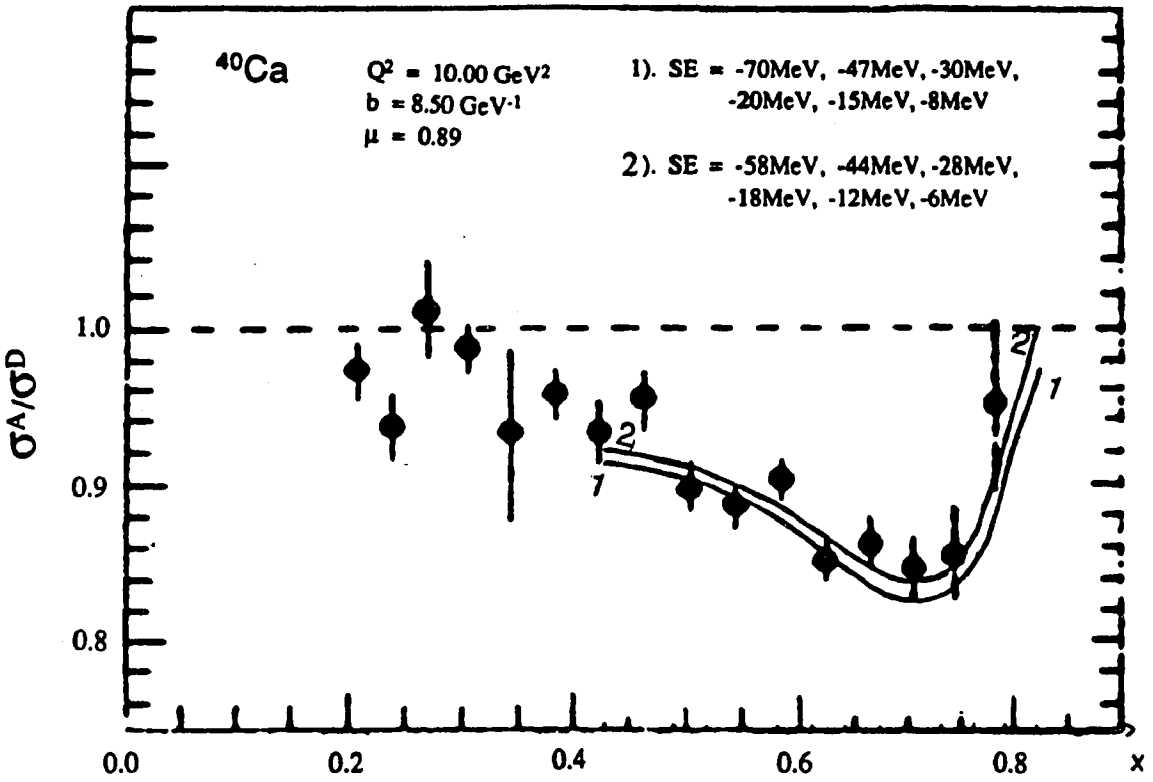

Same caption as Fig. 12. except that the target is ^{40}Ca. Here b = 8.5 GeV^{-1}, μ = 0.89 GeV. The separation energies used were:

1) $\varepsilon(1s_{1/2}) = 70$ MeV, $\varepsilon(1p_{3/2}) = 47$ MeV, $\varepsilon(1p_{1/2}) = 30$ MeV, $\varepsilon(1d_{5/2}) = 20$ MeV, $\varepsilon(2s_{1/2}) = 15$ MeV, $\varepsilon(1d_{3/2}) = 8$ MeV

with a mean value, $<\varepsilon> = 28.5$ MeV and

2) $\varepsilon(1s_{1/2}) = 58$ MeV, $\varepsilon(1p_{3/2}) = 44$ MeV, $\varepsilon(1p_{1/2}) = 28$ MeV, $\varepsilon(1d_{5/2}) = 18$ MeV, $\varepsilon(2s_{1/2}) = 12$ MeV, $\varepsilon(1d_{3/2}) = 6$ MeV

Figure 13

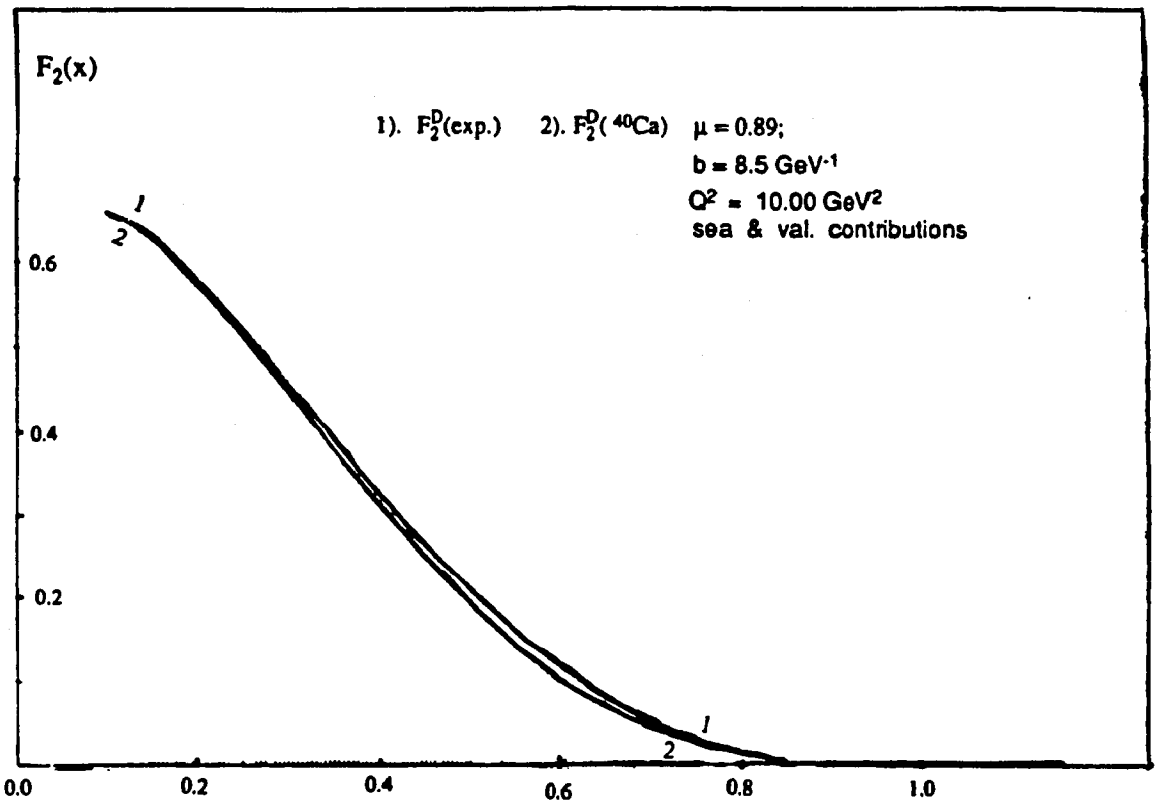

Curve (1) presents the (averaged) experimental values of $F_2^D(x)$ used in this work. (See Refs. 40 and 55.) Curve (2) represents the structure function calculated for ^{40}Ca, when we include the model of the 'sea' described in Sec. 3.13. The parameters μ and b are the same as in the caption to Fig. 13. We use the first set of separation energies given in that caption.

Figure 14.

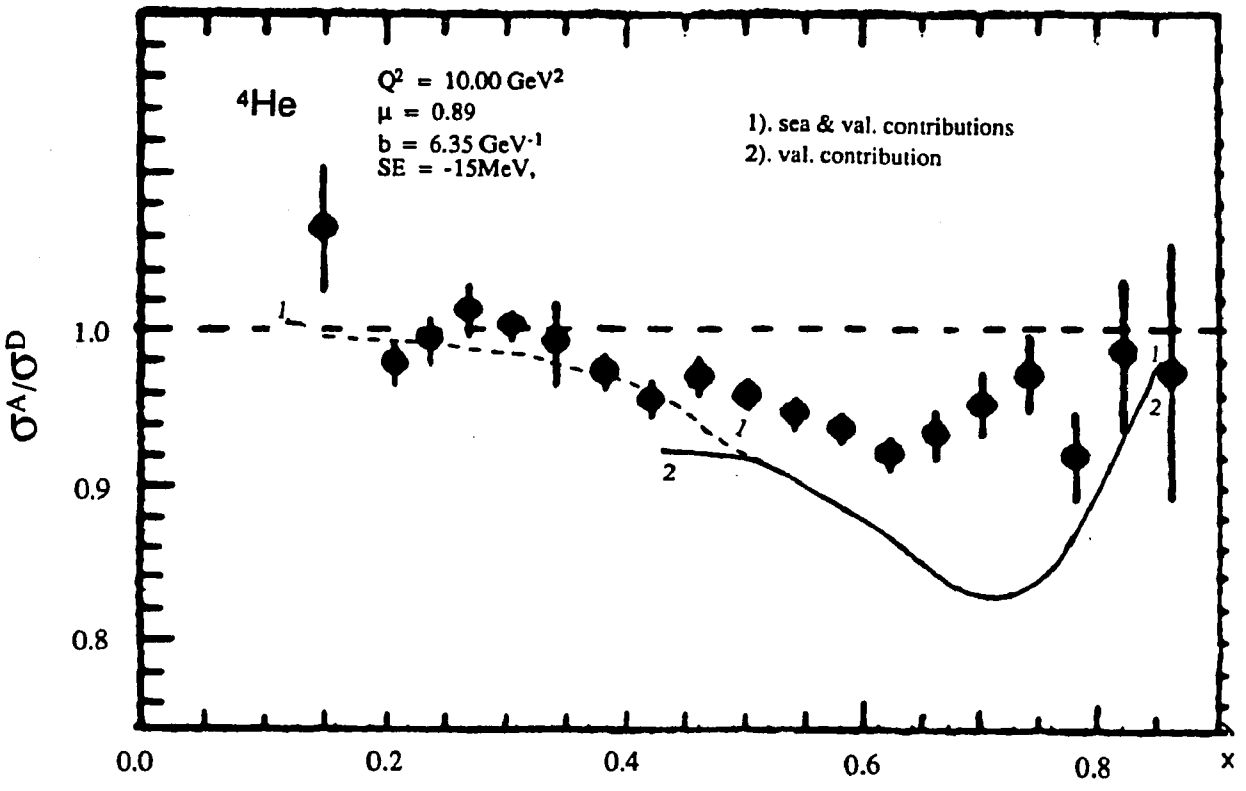

Same caption as that of Fig. 11, except that the contribution of the 'sea' is included using the model of Sec. 3.1.3 in the result shown as a dashed line. The solid line is the result without the 'sea' contribution and was shown previously in Fig.11. Note that the 'sea' contribution is quite small beyond $x_t \approx 0.5$, so that the previous result is unmodified for the larger values of x. (Here $\varepsilon(1s_{1/2}) = 15$ MeV.)

Figure 15

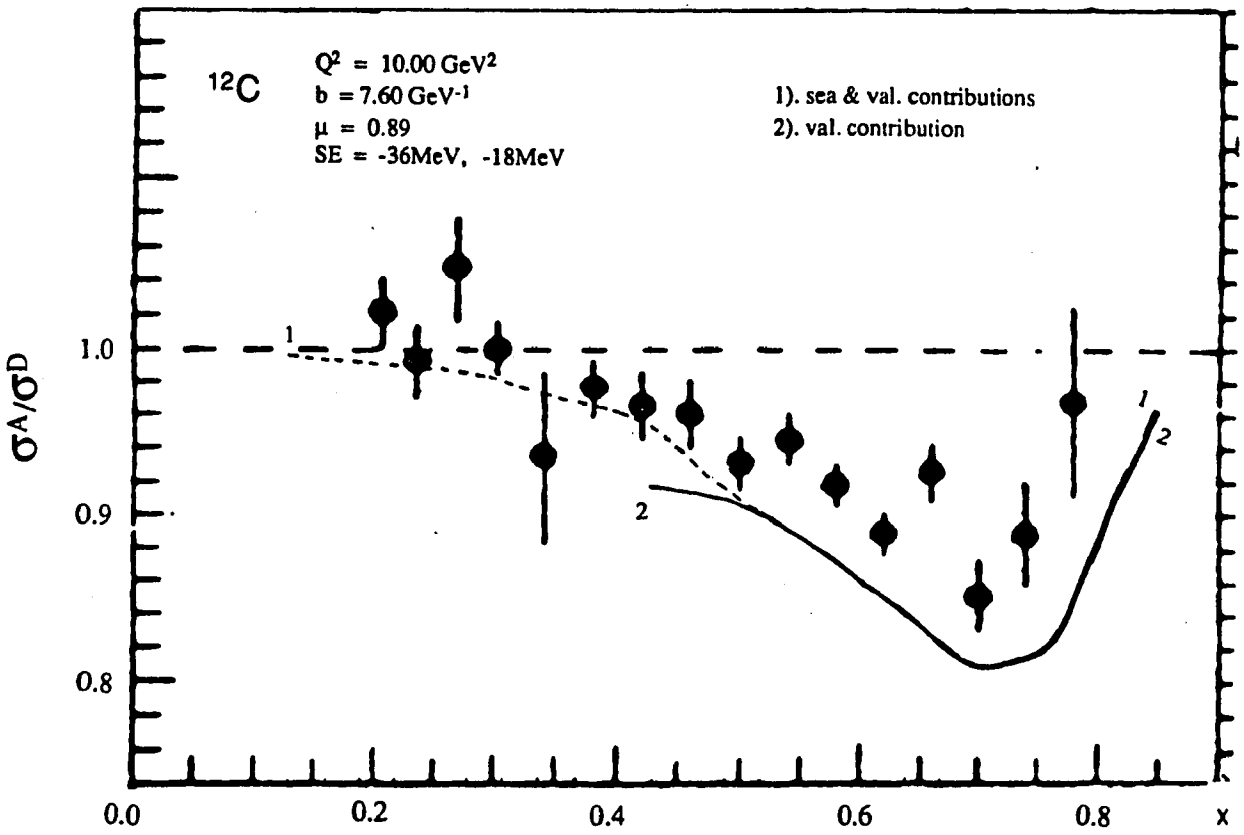

Similar caption as that of Fig. 15, except that the target is ^{12}C. The parameters μ and b for ^{12}C are those given in the caption to Fig. 12. (Here $\varepsilon(1s_{1/2}) = 36$ MeV and $\varepsilon(1p_{3/2}) = 18$ MeV.) The solid line is the result obtained without the 'sea' contribution and was shown previously in Fig. 12.

Figure 16

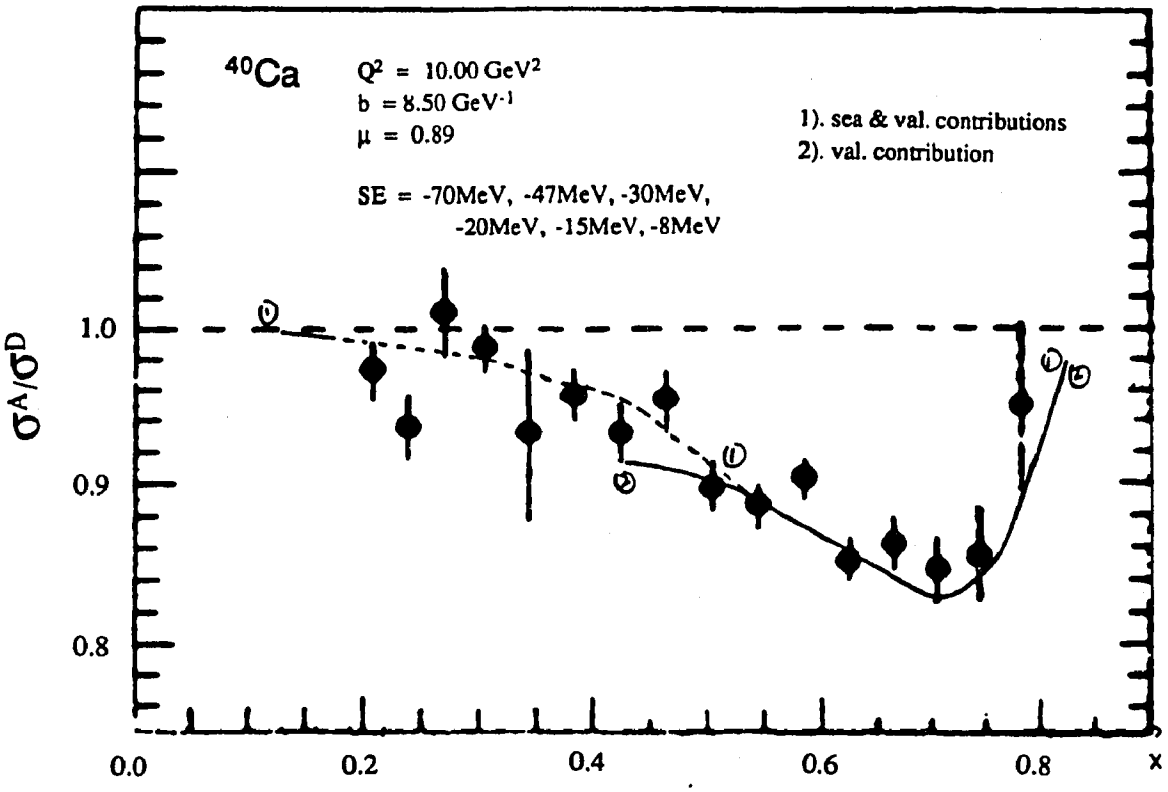

Similar caption as that of Fig. 16, except that the target is ^{40}Ca. The parameters μ and b are given in the caption to Fig. 13; the first set of separation energies given there was used. The solid line is the result obtained without inclusion of the sea contribution.

Figure 17

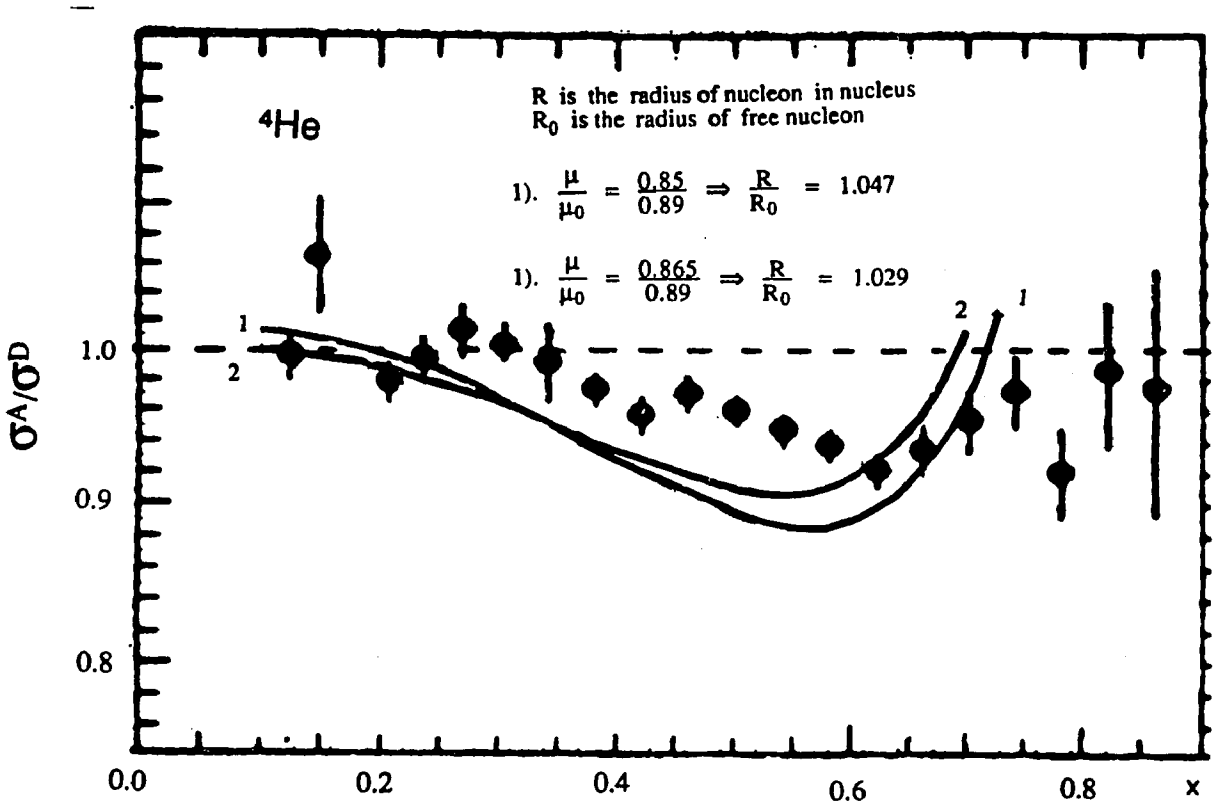

The solid line shows the ratio of the (averaged) structure function to the experimental data[40] for the structure function of the deuteron. The calculation was made for ^{4}He by using the experimental data[40] and including the 'swollen nucleon' effect. The deuteron data is averaged over several values of Q^2, as in Ref. 55. The result is shown for two different μ's, (corresponding to different radii of the nucleon in the nucleus.)

1). $\mu = 0.85$, 2). $\mu = 0.865$.

Figure 18

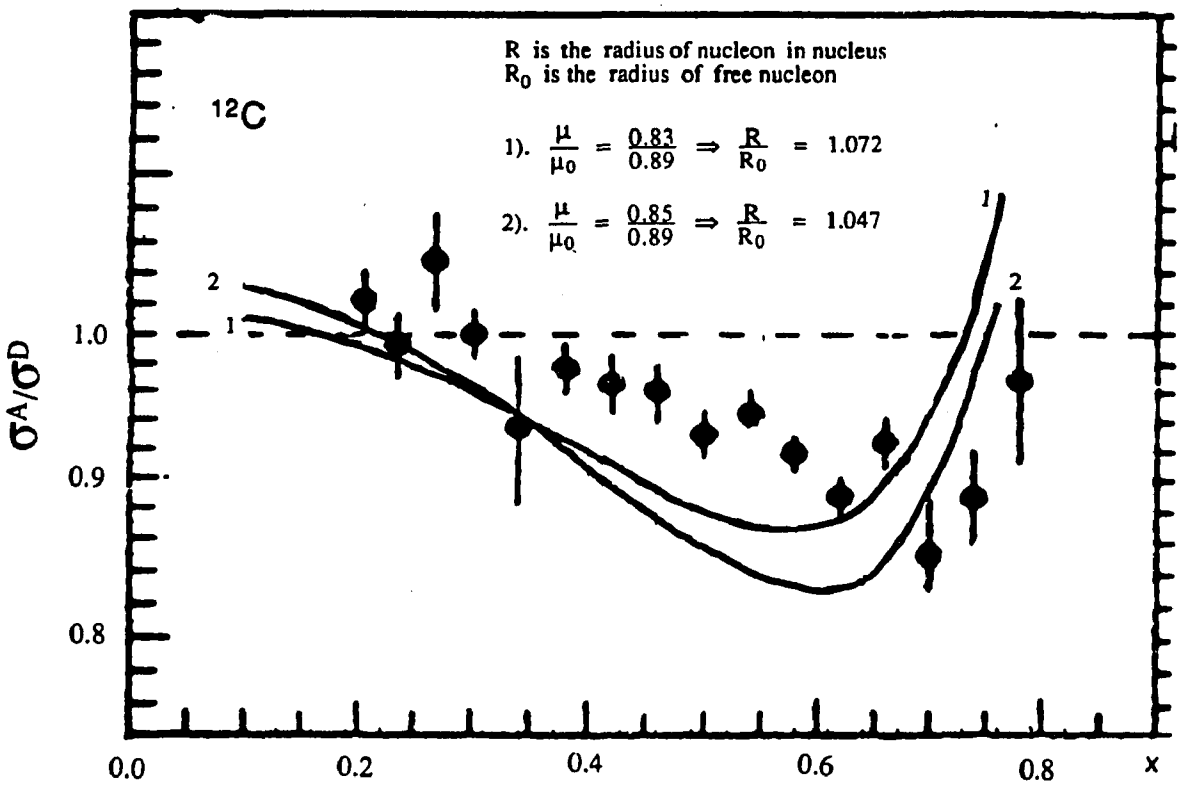

Same caption as Figure 18, except that the target is ^{12}C. Results are given for two choices of μ.

1). $\mu = 0.83$ 2). $\mu = 0.85$

Figure 19

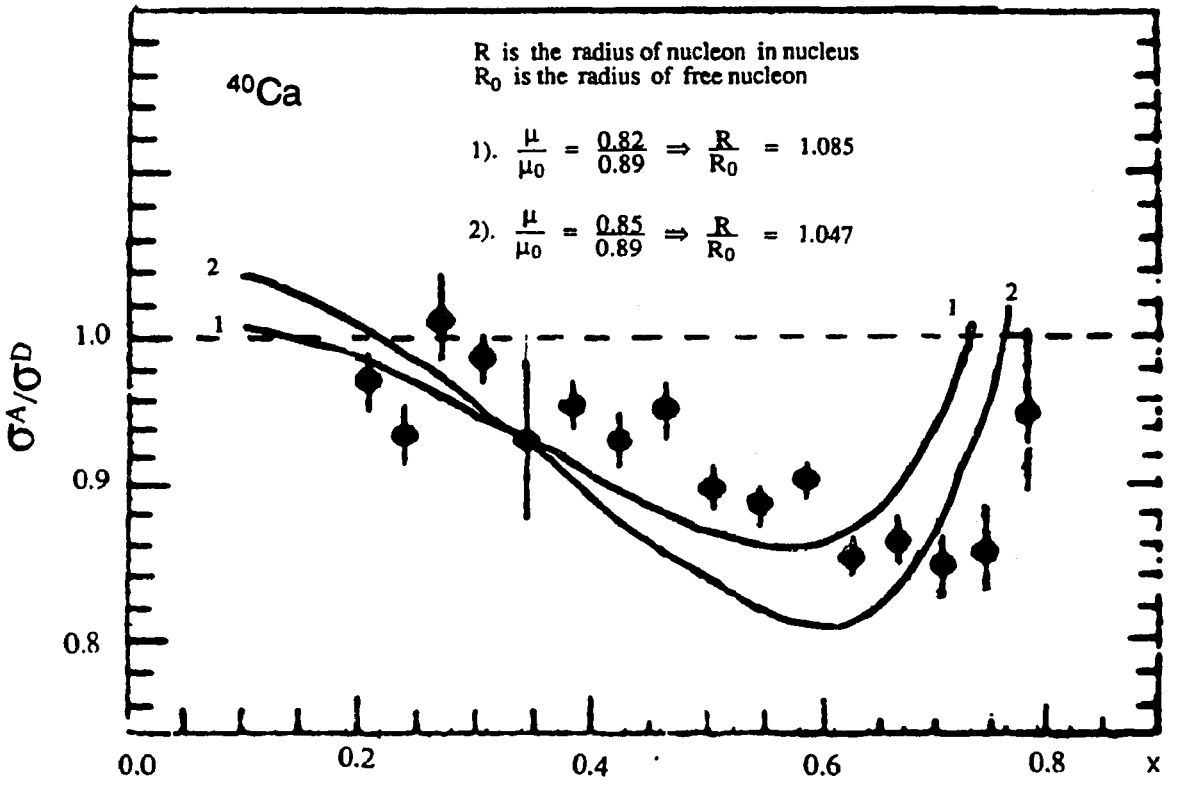

Same caption as Figure 19, except that the target is ^{40}Ca. Results are given for two choices of μ.

1). $\mu = 0.82$ 2). $\mu = 0.85$

Figure 20

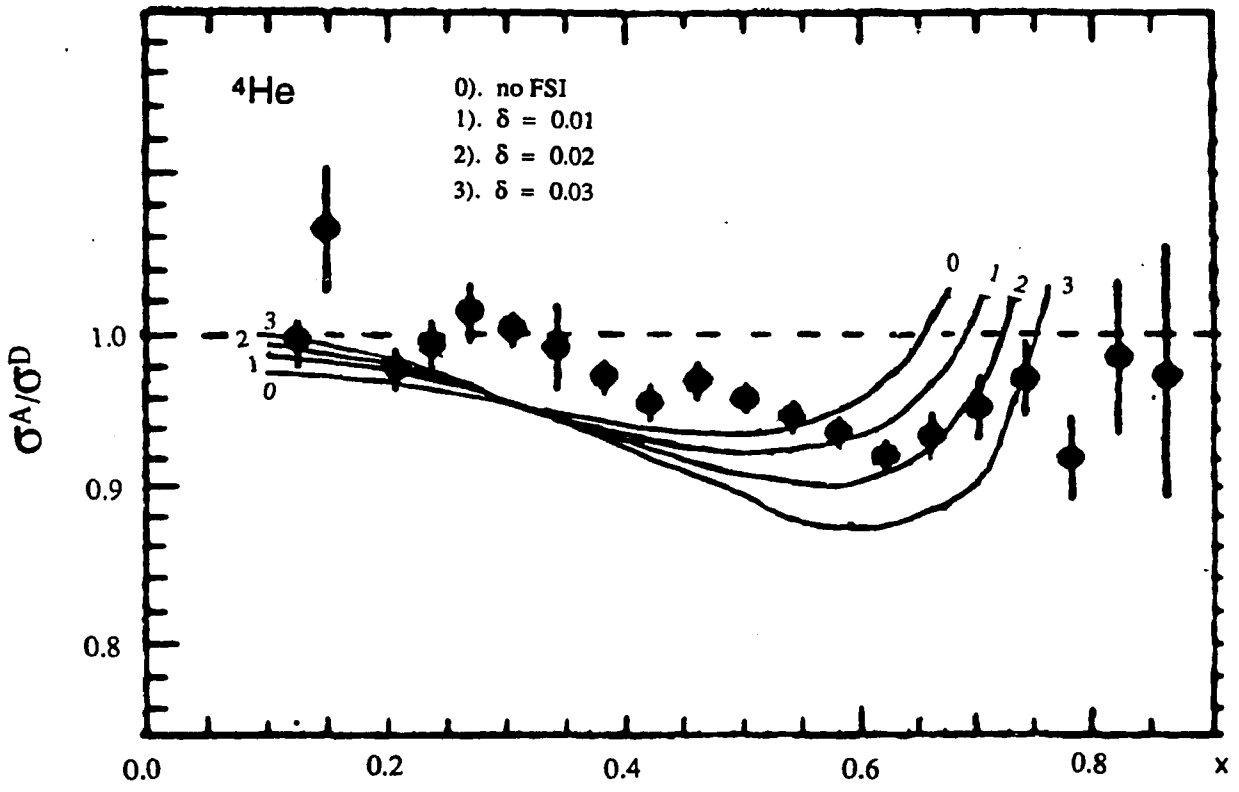

The solid line shows the ratio of the (averaged) structure function to the experimental data[40] for the structure function of deuteron. The calculation is made for ^{4}He by using the experimental data[40] for the structure function and includes the final state interaction effect. The deuteron data is averaged over several values of Q^2, as in Ref. 55. The result is shown for four different values of δ, the fraction of momentum lost.

0). δ = 0.0 (no FSI), 1). δ = 0.01,

2). δ = 0.02, 3). δ = 0.03.

Figure 21

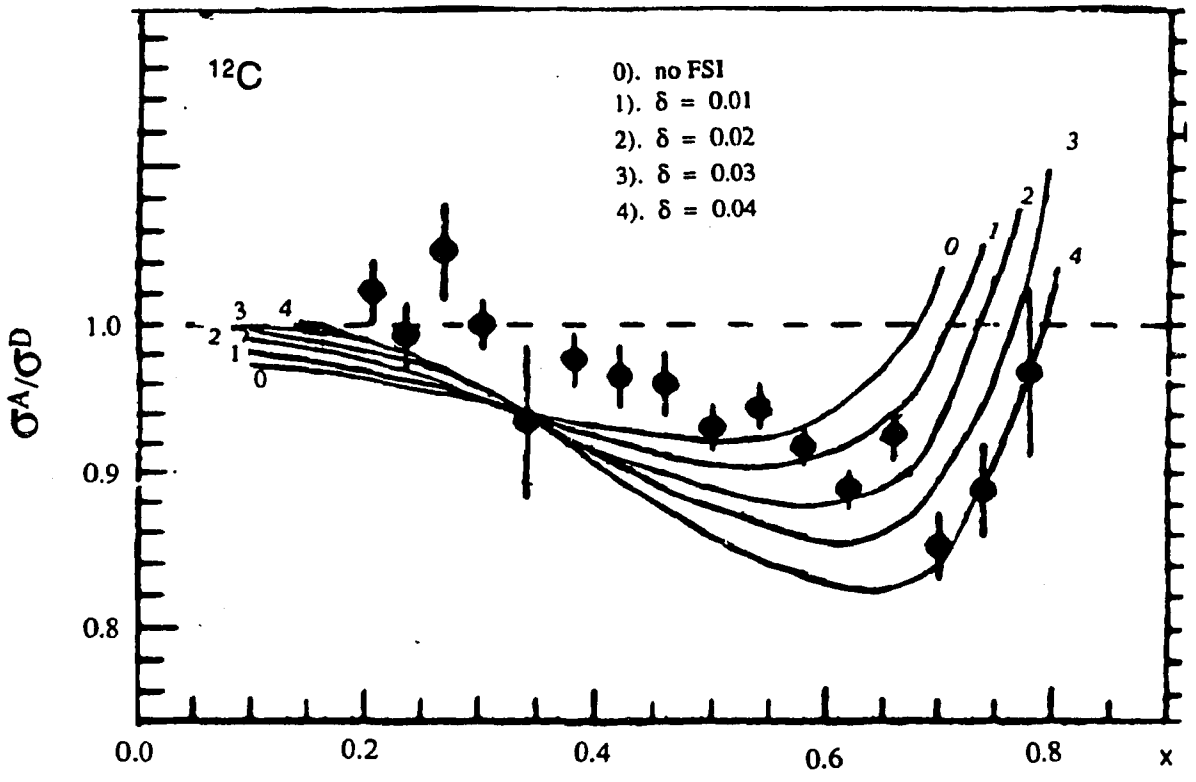

Same caption as Figure 21, except that the target is ^{12}C. Results are given for five choices of the δ value.

0). δ = 0.0 (no FSI), 1). δ = 0.01, 2). δ = 0.02,
3). δ = 0.03, 4). δ = 0.04.

Figure 22

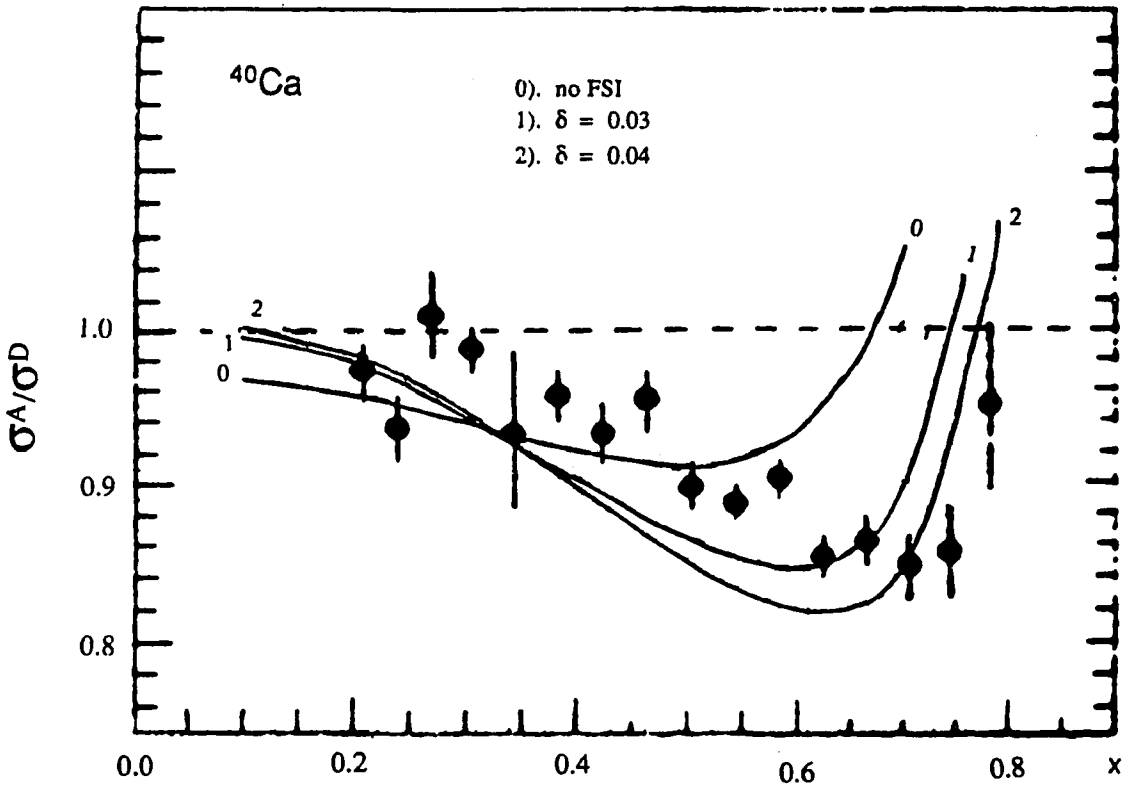

Same caption as Figure 21, except that the target is ^{12}C. Results are given for three choices of δ.

0). δ = 0.0 (no FSI), 1). δ = 0.03, 2). δ = 0.04

Figure 23

Figure 24. Values of $\Delta(A, Q^2)$ obtained in our analysis are shown for three values of Q^2,

a). $Q^2 = 5\,GeV^2$,

b). $Q^2 = 10\,GeV^2$,

c). $Q^2 = 15\,GeV^2$.

The series of dots represent the nuclei studied with mass numbers: A = 4, 9, 12, 27, 40, 56, 108 and 197. The uncertainties in the values of Δ shown in the figure are discussed in the text.

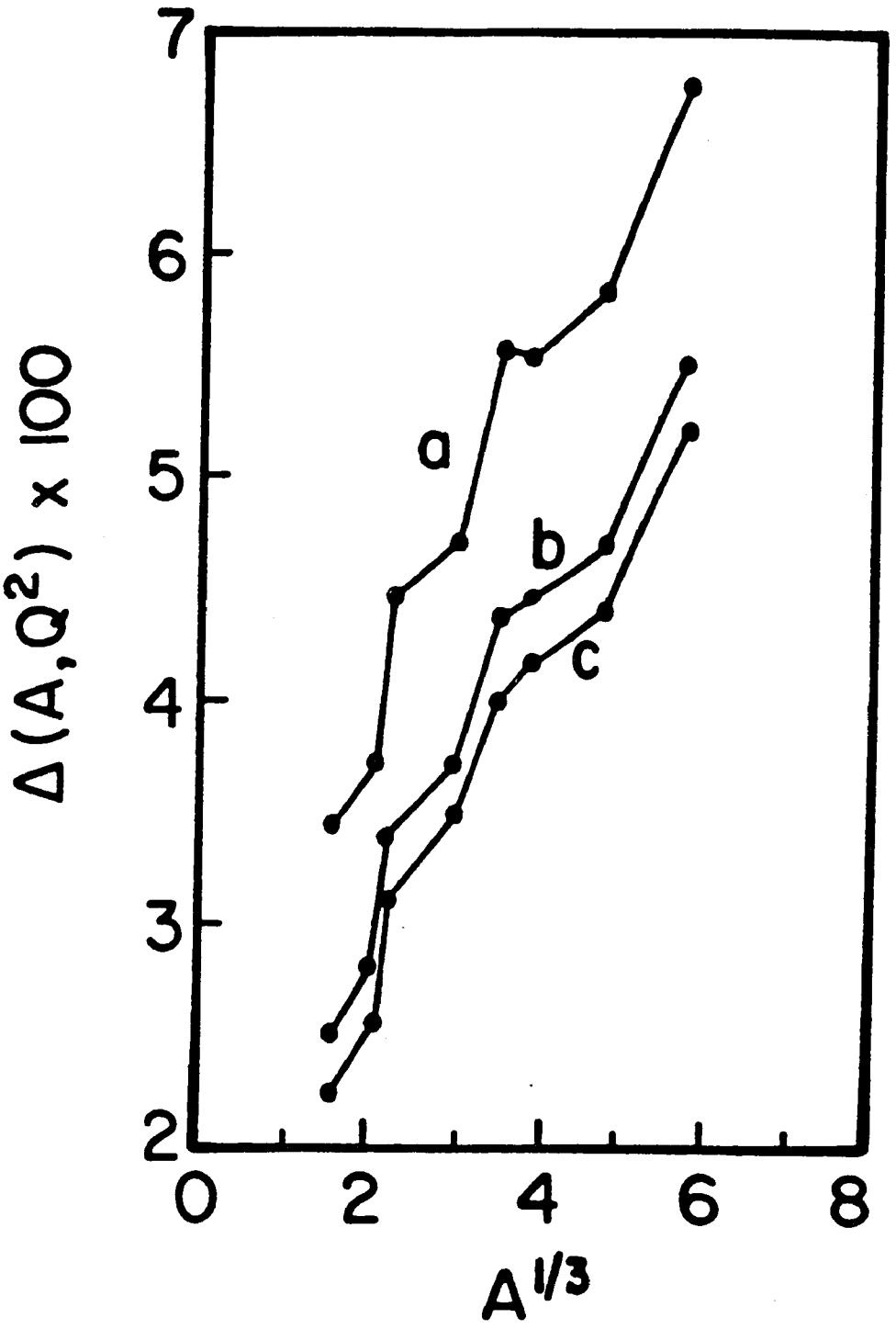

Figure 24

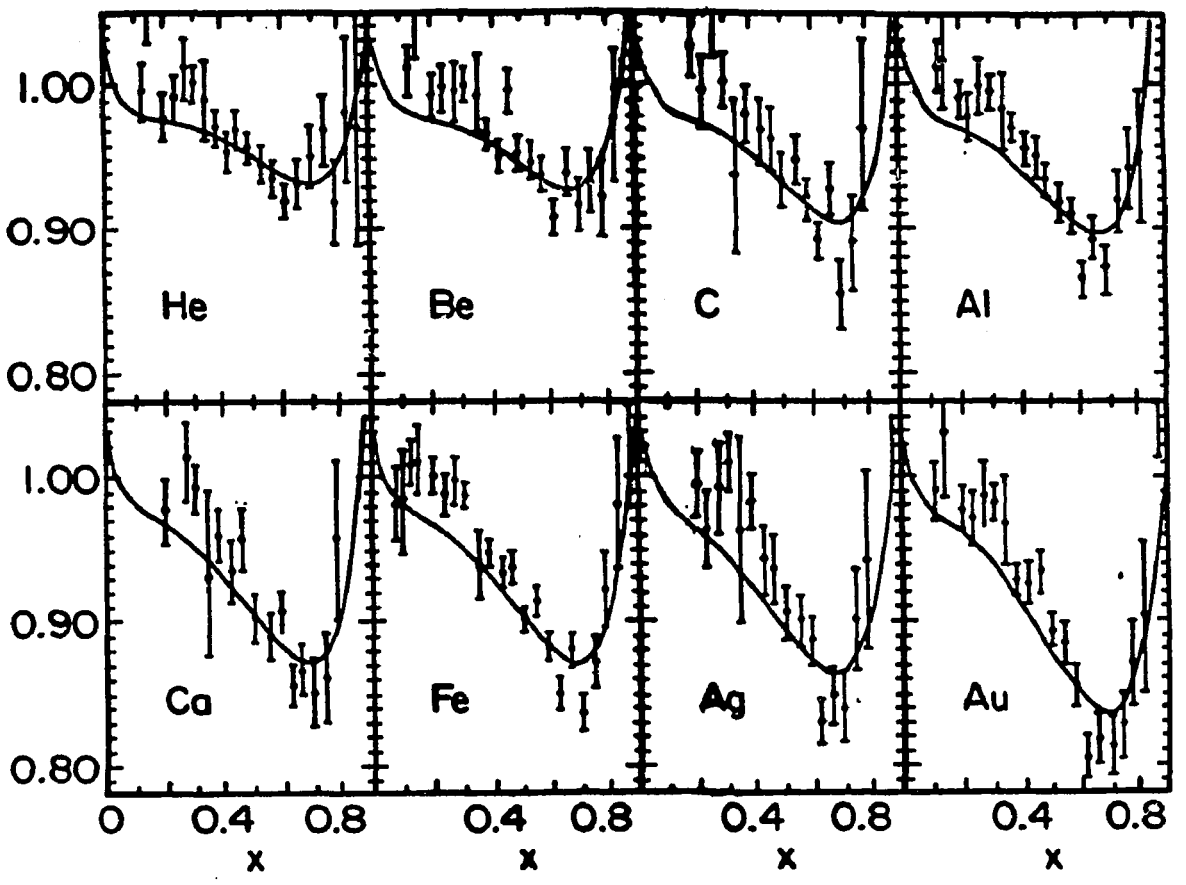

The analysis described in the text yields the figures shown, if nucleon and deuteron structure functions at $Q^2 = 10\,GeV^2$ are used. Corresponding values of Δ are given in curve b) of figure 24. (The data is taken from Ref. 47.) Fits of slightly larger χ^2 are obtained at $Q^2 = 5$ and $15\,GeV^2$. These fits correspond to curves a) and c) of Fig. 24, respectively.

Figure 25

Appendix A

For convenience, we neglect superscripts A.

$$W_{\mu\nu} = (-g_{\mu\nu} + \frac{q_\mu q_\nu}{q^2}) W_1 + \frac{\hat{P}_\mu \hat{P}_\nu}{P^2} W_2 ,$$

where

$$\hat{P}_\mu = P_\mu - (P\cdot q) q_\mu / q^2 .$$

From $W_{\mu\nu}$, we can form two Lorentz invariants:

$$I_1 = W_{\mu\nu} \hat{P}^\mu \hat{P}^\nu$$

$$= (-g_{\mu\nu} + \frac{q_\mu q_\nu}{q^2}) \hat{P}^\mu \hat{P}^\nu W_1 + \frac{\hat{P}_\mu \hat{P}_\nu}{P^2} \hat{P}^\mu \hat{P}^\nu W_2 ,$$

$$= - W_1 \hat{P}^2 + W_2 \frac{\hat{P}^4}{P^2} .$$

$$I_2 = W^\mu{}_\mu ,$$

$$= (- g^\mu{}_\mu + \frac{q^\mu q_\mu}{q^2}) W_1 + \frac{\hat{P}^\mu \hat{P}_\mu}{P^2} W_2 ,$$

$$= -3W_1 + \frac{\hat{P}^2}{P^2} W_2 .$$

From I_1 and I_2, we can solve W_1 and W_2,

$$W_1 = \frac{1}{2\hat{P}^2}(I_1 - \hat{P}^2 I_2),$$

$$= -\frac{1}{2}(I_2 - \frac{I_1}{\hat{P}^2}),$$

$$= -\frac{1}{2}(g^{\mu\nu} - \frac{\hat{P}^\mu \hat{P}^\nu}{\hat{P}^2}) W_{\mu\nu} .$$

$$W_2 = \frac{P^2}{2\hat{P}^4}(3I_1 - \hat{P}^2 I_2),$$

$$= -\frac{P^2}{2\hat{P}^2}(I_2 - \frac{3I_1}{\hat{P}^2}),$$

$$= -\frac{m^2}{2\hat{P}^2}(g^{\mu\nu} - \frac{3\hat{P}^\mu \hat{P}^\nu}{\hat{P}^2}) W_{\mu\nu} . \qquad (\text{When } P^2 = m^2.)$$

Appendix B

$$W^N_{\mu\nu}(P,q) = \left(-g_{\mu\nu} + \frac{q_\mu q_\nu}{q^2}\right) W^N_1 + \frac{\hat{P}_\mu \hat{P}_\nu}{P^2} W^N_2 ,$$

and

$$W^A_{\mu\nu}(P_A, q) = \sum_{i=1}^{A} \int d^3P \left|\phi_i(\vec{P})\right|^2 W^N_{\mu\nu}(P, q) .$$

For convenience, we neglect superscripts N in $W^N_{\mu\nu}$, W^N_1 and W^N_2 . So,

$$W^A_1 = -\frac{1}{2}\left(g^{\mu\nu} - \frac{\hat{P}^\mu_A \hat{P}^\nu_A}{\hat{P}^2_A}\right) W^A_{\mu\nu} ,$$

$$= -\frac{1}{2}\sum_{i=1}^{A} \int d^3P \left|\phi_i(\vec{P})\right|^2 \left(g^{\mu\nu} - \frac{\hat{P}^\mu_A \hat{P}^\nu_A}{\hat{P}^2_A}\right)\left[\left(-g_{\mu\nu} + \frac{q_\mu q_\nu}{q^2}\right) W_1 + \frac{\hat{P}_\mu \hat{P}_\nu}{P^2} W_2\right] .$$

In which,

$$\left(g^{\mu\nu} - \frac{\hat{P}^\mu_A \hat{P}^\nu_A}{\hat{P}^2_A}\right)\left(-g_{\mu\nu} + \frac{q_\mu q_\nu}{q^2}\right) W_1 = \left(-g^\mu{}_\mu + \frac{\hat{P}^\mu_A \hat{P}^\nu_A g_{\mu\nu}}{\hat{P}^2_A} + \frac{g^{\mu\nu} q_\mu q_\nu}{q^2}\right) W_1 ,$$

$$= (-4 + 1 + 1) W_1 = -2W_1 .$$

Because

$$\hat{P}^2 = [P^\mu - (P\cdot q)q^\mu/q^2 \,||\, P_\mu - (P\cdot q)q_\mu/q^2] ,$$

$$= P^2 - \frac{(P\cdot q)^2}{q^2} \quad .$$

Similarly, we have

$$\widehat{P}_A^2 = P_A^2 - \frac{(P_A\cdot q)^2}{q^2} \quad .$$

In the target rest frame,

$$\widehat{P}_A^2 = M_A^2 - \frac{M_A^2\,\nu^2}{q^2} \quad ,$$

$$= M_A^2\,(1 - \frac{\nu^2}{q^2}) = -M_A^2\frac{\vec{q}^2}{q^2} \quad ,$$

and

$$\widehat{P}\cdot\widehat{P}_A = [P^\mu - (P\cdot q)q^\mu/q^2\,][\,P_{A\mu} - (P_A\cdot q)q_\mu/q^2\,] \quad ,$$

$$= P\cdot P_A - \frac{(P\cdot q)\,(P_A\cdot q)}{q^2} \quad ,$$

$$= M_A[\,p_0 - \frac{\nu(P\cdot q)}{q^2}\,] \quad .$$

Thus,

$$(g^{\mu\nu} - \frac{\widehat{P}_A^\mu\widehat{P}_A^\nu}{\widehat{P}_A^2})\frac{\widehat{P}_\mu\widehat{P}_\nu}{P^2}W_2 = [\,\widehat{P}^2 - \frac{(\widehat{P}\cdot\widehat{P}_A)^2}{\widehat{P}_A^2}\,]\frac{W_2}{P^2} \quad ,$$

$$= \left(P^2 - \frac{(P\cdot q)^2}{q^2} + \frac{q^2}{\vec{q}^2}[\,p_0 - \frac{\nu(P\cdot q)}{q^2}\,]^2\right)\frac{W_2}{P^2} \quad ,$$

$$= \left(P_0^2 - \vec{P}^2 + \frac{q^2}{\vec{q}^2} P_0^2 - \frac{(P\cdot q)^2}{q^2} - \frac{2P_0\nu(P\cdot q)}{\vec{q}^2} + \frac{\nu^2(P\cdot q)^2}{\vec{q}^2 q^2} \right) \frac{W_2}{P^2} ,$$

$$= \left(\frac{\nu^2}{\vec{q}^2} P_0^2 - \vec{P}^2 - \frac{(P\cdot q)^2}{\vec{q}^2} - \frac{2P_0\nu(P\cdot q)}{\vec{q}^2} \right) \frac{W_2}{P^2} ,$$

$$= \left(\frac{1}{\vec{q}^2} [P_0\nu - (P\cdot q)]^2 - \vec{P}^2 \right) \frac{W_2}{P^2} ,$$

$$= [\frac{1}{\vec{q}^2} (\vec{P}\cdot\vec{q})^2 - \vec{P}^2] \frac{W_2}{P^2} ,$$

$$= [(\vec{P}\cdot\hat{q})^2 - \vec{P}^2] \frac{W_2}{P^2} ,$$

$$= - P_\perp^2 \frac{W_2}{P^2} .$$

Therefore,

$$W_1^A = -\frac{1}{2} (g^{\mu\nu} - \frac{\hat{P}_A^\mu \hat{P}_A^\nu}{\hat{P}_A^2}) W_{\mu\nu}^A ,$$

$$= -\frac{1}{2} \sum_{i=1}^{A} \int d^3P \left|\phi_i(\vec{P})\right|^2 \left[-2 W_1 - \frac{P_\perp^2}{P^2} W_2 \right] ,$$

$$= \sum_{i=1}^{A} \int d^3P \left|\phi_i(\vec{P})\right|^2 \left[W_1 + \frac{P_\perp^2}{2P^2} W_2 \right] .$$

$$W_2^A = -\frac{1}{2}\frac{M_A^2}{\hat{P}_A^2}\left(g^{\mu\nu} - \frac{3\,\hat{P}_A^\mu\,\hat{P}_A^\nu}{\hat{P}_A^2}\right)W_{\mu\nu}^A \ .$$

$$= -\frac{1}{2}\sum_{i=1}^{A}\int d^3P\left|\phi_i(\vec{P})\right|^2\frac{M_\Lambda^2}{\hat{P}_\Lambda^2}\left[g^{\mu\nu} - \frac{3\,\hat{P}_\Lambda^\mu\,\hat{P}_\Lambda^\nu}{\hat{P}_\Lambda^2}\right]\left[\left(-g_{\mu\nu} + \frac{q_\mu q_\nu}{q^2}\right)W_1 + \frac{\hat{P}_\mu\hat{P}_\nu}{P^2}\,W_2\right].$$

where,

$$\left[g^{\mu\nu} - \frac{3\,\hat{P}_A^\mu\,\hat{P}_A^\nu}{\hat{P}_A^2}\right]\left(-g_{\mu\nu} + \frac{q_\mu q_\nu}{q^2}\right)W_1 = (-4 + 1 + 3)\,W_1 = 0 \ .$$

and

$$\frac{M_A^2}{\hat{P}_A^2}\left[g^{\mu\nu} - \frac{3\,\hat{P}_A^\mu\,\hat{P}_A^\nu}{\hat{P}_A^2}\right]\frac{\hat{P}_\mu\hat{P}_\nu}{P^2}\,W_2 = \frac{M_A^2}{P^2}\frac{1}{\hat{P}_A^2}\left[\hat{P}^2 - \frac{3\,(\hat{P}\cdot\hat{P}_A)^2}{\hat{P}_A^2}\right]W_2 \ .$$

$$= -\frac{1}{P^2}\frac{q^2}{\vec{q}^2}\left[\hat{P}^2 - \frac{(\hat{P}\cdot\hat{P}_A)^2}{\hat{P}_A^2} - \frac{2\,(\hat{P}\cdot\hat{P}_A)^2}{\hat{P}_A^2}\right]W_2 \ .$$

$$= -\frac{1}{P^2}\frac{q^2}{\vec{q}^2}\left[-P_\perp^2 - \frac{2\,(\hat{P}\cdot\hat{P}_A)^2}{\hat{P}_A^2}\right]W_2 \ .$$

Further, we have

$$- \frac{q^2}{\vec{q}^2} \frac{(\hat{P} \cdot \hat{P}_A)^2}{\hat{P}_A^2} = \frac{q^2}{\vec{q}^2} \left(\frac{q^2}{\vec{q}^2} \left[P_0 - \frac{\nu (P \cdot q)}{q^2} \right]^2 \right) ,$$

$$= \frac{q^2}{\vec{q}^4} \left[q^2 P_0^2 + \frac{\nu^2 (P \cdot q)^2}{q^2} - 2\nu (P \cdot q) \right] ,$$

$$= \frac{q^2}{\vec{q}^4} \left(- \vec{q}^2 P_0^2 + (\vec{P} \cdot \vec{q})^2 + \frac{\vec{q}^2}{q^2} \left[P_0^2 \nu^2 + (\vec{P} \cdot \vec{q})^2 - 2 P_0 \nu (\vec{P} \cdot \vec{q}) \right] \right) ,$$

$$= \frac{1}{\vec{q}^4} \left[\vec{q}^4 P_0^2 + \nu^2 (\vec{P} \cdot \vec{q})^2 + 2 P_0 \nu \vec{q}^2 (\vec{P} \cdot \vec{q}) \right] .$$

Since, we have $q = (\nu, 0, 0, q_3)$, $\vec{q}^2 = q_3^2$ and $Q^2 = - q^2$,

$$- \frac{q^2}{\vec{q}^2} \frac{(\hat{P} \cdot \hat{P}_A)^2}{\hat{P}_A^2} = \frac{1}{q_3^2} \left[q_3^2 P_0^2 + \nu^2 P_3^2 - 2 P_0 \nu P_3 q_3 \right] ,$$

$$= \frac{1}{q_3^2} (P^0 q^3 - P^3 q^0)^2 .$$

Thus,

$$W_2^A = -\frac{1}{2}\frac{M_A^2}{\hat{P}_A^2}\left[g^{\mu\nu} - \frac{3\,\hat{P}_A^\mu \hat{P}_A^\nu}{\hat{P}_A^2}\right]\frac{\hat{P}_\mu \hat{P}_\nu}{P^2}\,W_2 \quad ,$$

$$= \sum_i \int d^3P \left|\phi_i(\vec{P})\right|^2 \left(\left[\frac{(P^0 q^3 - P^3 q^0)}{q^3}\right]^2 + \frac{P_\perp^2}{2}\left[\frac{Q^2}{(q^3)^2}\right]\right)\frac{W_2^N}{P^2} \quad .$$

References

1. S. Dasu, Phys. Rev. Lett. 64, 2591(1988).

2. J. J. Aubert et al., Phys. Lett. 123B, 275(1983).

3. A. Bodek et al., Phys. Rev. Lett. 50, 1431, 51, 534(1983); R. G. Arnold et al., Phys. Rev. Lett. 52, 727(1983).

4. G. Bari et al., Phys. Lett. 163B, 282(1985).

5. H. Abramowicz et al., Z. Phys. C25, 29(1984); See also M. A. Parker et al., Nucl. Phys. B232, 1(1984); A. M. Cooper et al., Phys. Lett. 141B 133(1984); J. Hanlon et al., Phys. Rev. D32, 2441(1985); V. V. Ammosov et al., JEPT Lett. 39, 393(1984); A. E. Asratian et al., Sov. J. Nucl. Phys. 43, 380(1986); WA25 and WA59 Collaboration, J. Guy et al., CERN Rep. CERN/EP86 - 217(Dec.1986). Submitted to Z. Phys. C

6. EMC Collaboation, P. Norton in XXIII Inf. Conf. on High Energy Physics, Berkeley, July, 1986, ed, S. C. Loken, (World Scientific, Singapore, 1987). P.1399

7. BCDMS Collaboration, A. C. Benvenuti et al., Phys. Lett. 189B, 483 (1987).

8. J. Ashman et al., Phys, Lett. 202B, 603(1988).

9. G. B. West, Ann. Phys. (NY)74, 464(1972).

10. R. L. Jaffe, in Relativistic Dynamics and Quark-Nuclear Physics, M. B. Johnson and A. Pickelsimer, eds.(Wiley, New York, 1986).

11. H. M. Jung, and G. A. Miller, Phys. Lett. 200B, 351(1988).

12. A. Bodek, and J. L. Ritchie, Phys. Rev. D23, 1070(1981).

13. G. V. Dunne, and A. W. Thomas, Phys. Rev. D33, 2061(1986); Nucl. Phys. A455, 701(1986).

14. L. L. Frankfurt, and M. I. Strikman, Phys. Rep. 76C 215(1981); Phys. Lett. 183B, 254(1987).

15. R. P. Bickerstaff, in Medium and High-Energy Nuclear Physics, ed. W-Y. P. Hwang, K.F.Liu and Y Tzeng (World Scientific,Singapore, 1989).

16. S. V. Akulinichev, S. A. Kulagin and G. M. Vagradov, Pis'ma, Zh. Eksp Teor. Fiz 42, 105(1985). (Engl. transl. JETP Lett. 42, 127, 1986); Phys. Lett. 158B, 485(1985); J. Phys. G: Nucl.Phys. 11L, 245(1985); S. V. Akulinichev, S. Shlomo, S. A. Kulagin and G. M. Vagladov, Phys. Rev. Lett. 55, 2239(1985).

17. W. B. Atwood and G. B. West, Phys. Rev. D7, 773(1973).

18. G. V. Dunne and A. W. Thomas, Nucl. Phys. A446, 437c(1985).

19. R. P. Bickerstaff and A.W. Thomas, Phys. Rev. D35, 108(1987).

20. C. A. Garcia-Canal, E. M. Santangelo, and H. Vucetich, Phys. Rev. Lett 53, 1430(1984).

21. G. L. Li, K. F. Liu and G. E. Brown, Phys. Lett. 213B, 531(1988).

22. C. H. Llewellyn-Smith, Phys. Lett. 128B, 107(1983).

23. M. Ericson and A. W. Thomas, Phys. Lett. 128B, 112(1983).

24. E. L. Berger, F. Coester and R. B. Wiringa, Phys. Rev. D29, 398(1984).

25. E. L. Berger and F. Coester, Phys. Rev. D32, 1071(1984); E. L. Berger and F. Coester in Quarks and Gluons in Particles and Nuclei ed. S. Brodsky and E. Moniz (World Scientific, Singapore) (1986); E. L. Berger and F. Coester in Ann. Rev. Nucl.Part. Sci. 37, 463 (1987).

26. F. Coester, in Quarks, Mesons and Nuclei, II, Electroweak Interaction, ed. W-Y. P. Hwang, and E. M. Henley (World Scientific, Singapore) (1988), p124.

27. T. A. Carey et al., Phys. Rev. Lett. 53, 144(1984).

28. O. Nachtmann and H. Pirner, Phys. Rev. C21, 277(1984).

29. F. E. Close, R. G. Roberts and G. Ross, Phys. Lett. 129B, 346(1983).

30. F. E. Close, R. L. Jaffe, R. G. Roberts and G. Ross, Phys. Rev. D31, 1004(1985).

31. R. L. Jaffe et al., Phys. Lett. 134B,449(1984).

32. R. L. Jaffe, Phys. Rev .Lett. 50, 228(1983).

33. I. Sick, Nucl. Phys. A434, 677(1985); Phys. Lett. 157B, 13(1985).

34. P. J. Mulders, Phys. Rev. Lett. 54, 2560(1985).

35. A. Krzywicki, Phys. Rev. D14, 152(1976).

36. P. Hoodbhoy and R. L. Jaffe, Phys. Rev. D35, 113(1987).

37. J. J. Aubert et al.,(EMC) Nucl. Phys. B259, 189(1985).

38. L. S. Celenza and C. M. Shakin, Phys. Rev. C27, 1561(1983); Erratum: Phys. Rev. C39, 2477(1989). This model is developed further, using more realistic wave functions in Ref. 39.

39. L. S. Celenza, A. Pantiziris, C. M. Shakin and H. W. Wang, Brooklyn College Reports: BCCNT 89/031/188(1989); BCCNT 89/041/190(1989); BCCNT 89/043/192(1989); BCCNT 89/051/193(1989); BCCNT 89/061/195(1989).

40. A. Bodek et al., Phys. Rev. D20, 1471(1979).

41. The relation between the nuclear binding analysis and the rescaling analysis is described in R. Bickerstaff and G. A. Miller Phys. Lett. 168B, 409(1986).

42. L. S. Celenza and C. M. Shakin, Phys. Rev. Lett. 27, 892(1984).

43. St. Glazek and C. M.Shakin, Brooklyn College Report: BBCNT 90/041/204(1990).

44. P. A. M. Dirac, Rev. Mod. Phys. 21, 392 (1949).

45. St. Glazek and M. Schaden, Zeit. f. Phys. A323, 451 (1985).

46. L. S. Osborne et al., Phys. Rev. Lett. 40, 1624 (1978); W. J.Womersley, Ph.D. Thesis (Oxford, 1986); PEGASYS proposal, (SLAC, Dec.1988 and Addendum, Oct. 1989) - K. Van Bibber (private communication).

47. R. G. Arnold et al., Phys. Rev. Lett. 52, 727 (1984); See also R. G. Anorold et al., SLAC-PUB-3257 (Nov. 1983, unpublished).

48. St. Glazek, Acta. Phys. Polon. B18, 85 (1987).

49. M. I. Strickman and L. L. Frankfurt, Phys. lett. B183, 254 (1987).

50. H. Uberall, Electron Scattering from Complex Nuclei, Part. A (Academic Press, New York, 1971). We use

$$K_F^A = (9\pi/8A)^{1/3}/R_A,$$

and choose R_A from values given on page 213 of this reference. (See Eqs.

(3.41g) and (3.41i).)

51. G. A. Miller, in Nuclera and Particle Physics on the Light Cone, Edit. M.B. Johnson and L. S. Kisslinger, (World Scientific, Singapore, 1989).

52. A. Bodek et al., Phys. Rev. D20, 105 (1979).

53. Particle Data Group, Rev. Mod. Phys. 56, S61 (1986)-Part II. J. Faltesse, Rapporteur talk at the XIV International Symposium on Lepton and Photon Interactions, Stanford, Aug. 6-12 (1989), published in Lepton and Photon Interactions at High Energies, Edited by M. Riordan (World Scientific, Singapore, 1990).

54. V. Landgraf, Plenary session, PANIC XII Conference, 1990.

55. R. G. Arnold, P. E. Bosted, C. C. Chang, J. Gomez, A. T. Katramatou, C. G. Petratos, A. A. Rahbar, S. E. Rook, A.F. Sill and Z.M.Szalata, A.Bodek, N. Giokaris, D. J. Sherden, B. A. Mecking and R. M. Lombard, Phys. Rev. Lett. 52, 727(1984).